REVIEW

Check for updates

Fabrication strategies for high quality halide perovskite films in solar cells

Xiangfan Xie, Shengqiao Zeng, Cangtao Zhou and Shuang Xiao (ID) *

Perovskite solar cell (PVSC) has emerged as a game-changing photovoltaic technique in recent years. Remarkable advances have been realized in its efficiency, stability, and large-scale fabrication techniques. High-quality halide perovskite films are the core component of PVSCs, which require suitable fabrication strategies. This review includes three key sections to provide a comprehensive overview of these strategies. First, we discuss the crystallization reaction-controlled growth of halide perovskite films from the aspects of intermediates and reaction conditions. Second, organic and inorganic additives are introduced to show their influence on film formation, as well as the underlying mechanism. Third, mass transfer-controlled growth of perovskite films is reviewed, including ion transfer and molecule transfer. Finally, the review is concluded by summing up the key points covered and discussions have been made about the potential routes for the further development of high-quality film fabrication strategies.

1. Introduction

Electricity generated from photovoltaics (PV) exceeded 1000 TW h in 2021, which was among the largest absolute generation of all renewable technologies worldwide.[1] From 2011 to 2021, PVs have grown at an average global rate of 30%, and PV modules prices have decreased by 40% for each doubling of the production capacity, which is becoming the lowest-cost option for renewable electricity generation around the world.[2] However, continuous reductions in costs per watt peak is not a foregone

Shenzhen Key Laboratory of Ultraintense Laser and Advanced Material Technology, Center for Advanced Material Diagnostic Technology, and College of Engineering Physics, Shenzhen Technology University, Shenzhen 518118, China. E-mail: xiaoshuang@sztu.edu.cn

conclusion as the leading commercial PV—silicon solar cells—have been reaching its theoretical limit of power conversion efficiency (PCE). Emerging PV technologies are highly required for improvements in the years to come.

Perovskite solar cells (PVSCs) have developed very rapidly in the past decade, of which the certified PCE has reached 26.1%, stability exceeds 3000 h, and active area surpasses 200 cm^2.[3–5] With such great achievements, PVSC has been regarded as a dark horse in the PV technology. The general formula of halide perovskites is ABX$_3$, where A is a monovalent cation [such as organic cations: $CH_3NH_3^+$ (MA$^+$), $CH_3(NH_2)_2^+$ (FA$^+$), or inorganic metal cation: cesium (Cs$^+$)], B is a divalent metal cation [such as lead (Pb^{2+}), tin (Sn^{2+}), and germanium (Ge^{2+})], and X is a monovalent halogen anion [such as iodide (I$^-$), bromide (Br$^-$),

Xiangfan Xie is a postgraduate student under the supervision of Prof. Shuang Xiao at College of Engineering Physics, Shenzhen Technology University. He obtained his BS degree from Sichuan University (2022). His current research is focused on perovskite X-ray detectors and perovskite–perovskite hetero-structures.

Xiangfan Xie

Shengqiao Zeng is currently an undergraduate student at Shenzhen Technology University. His research focuses on the synthesis of halide perovskites, X-ray detectors, and semiconductor heterojunctions.

Shengqiao Zeng

and chloride (Cl⁻)].[6–11] Benefiting from the hybrid composition, halide perovskites exhibit excellent properties such as adjustable band gap, high carrier mobility, large optical absorption coefficient, small exciton binding energy, and solution processability.[12–17] These properties are crucial to achieve high performance and low cost solar cells.

To realize the above properties, high quality halide perovskite films should be synthesized, which requires effective strategies for film deposition.[18,19] The formation of halide perovskites in precursors is a chemical process, which is highly related to the crystal growth.[20] It could be soon recognized that adjusting the crystallization reactions of halide perovskites might be an effective way to manipulate their growth process and even the film quality. Indeed, various powerful strategies have been developed, which are based on controlling the chemical reactions for halide perovskite formation.[21–23] With these strategies, perovskite films could exhibit large grain sizes, flat and compact surfaces, low defect density, long carrier lifetime, and good stability.[6,24–31] The PVSCs fabricated with these films have achieved record PCE and passed IEC61215 specifications, which make it possible to manufacture highly performed, stable, and low-cost PV products in industries.[4,32,33] Therefore, it is important to review the fabrication strategies for high-quality halide perovskite films, including the aspect of crystallization reaction-controlled growth.

The main part of this review is divided into three sections. In the "crystallization reaction-controlled growth" section, we summarize the methods to adjust the reaction activity for high-quality perovskite films *via* intermediate engineering. Then, typical reaction conditions are discussed to show the influence of temperature, precursor concentration, and pressure toward film growth. In the "additive-controlled growth" section, we summarize the representative organic and inorganic additives. Meanwhile, the mechanism of additive-controlled growth of perovskite films is discussed. In the "mass transfer-controlled growth", we introduce typical methods to improve the quality of perovskite films by controlling ion and molecule transfer in the film formation process. Finally, we summarize the review and provide perspectives for future developments in this exciting area.

2. Crystallization reaction-controlled growth

In this section, we summarized and discussed the typical methods for synthesizing perovskite films, which are controlled by crystallization reactions. These methods can be divided into two categories: intermediate engineering and reaction conditions. In the "intermediates engineering" part, we discussed intermediate-controlled perovskite growth. In the "reaction conditions" part, we discussed the influence of reaction temperature, pressure, and precursor concentration.

2.1 Intermediate engineering

At present, most PVSCs with outstanding performance have been fabricated by solution-based methods.[34–40] To achieve this, tremendous efforts have been undertaken to improve these classical and universal strategies, which yields several important progresses. Before introducing details of each method, the chemical routes of intermediate conversion should be discussed, which could facilitate the understanding of advanced solution-based methods.

When the solute is dissolved in solution and forms a precursor solution, some solute molecules and solvent molecules will bind with each other to form adducts, which are called as Lewis adducts.[18,20,41] This concept comes from the Lewis acid–base theory. In this theory, a base is defined as an electron-pair donor, and an acid is defined as an electron-pair acceptor. They can easily have chemical interaction to form adducts and share electrons. In short, the intermediate can be defined as a complex, which is formed by the interaction between perovskite precursors and small molecules.[42] For example, the usually used molecules with Lewis-base feature

Cangtao Zhou is a chair professor at the Center for Advanced Material Diagnostic Technology, and College of Engineering Physics, Shenzhen Technology University. His current research interests include new particle accelerators driven by ultra-intense lasers, ultrafast precision diagnosis technology, large-scale computer simulation in high-energy-density physics, high power pulse laser loading technology, and extreme matter.

Cangtao Zhou
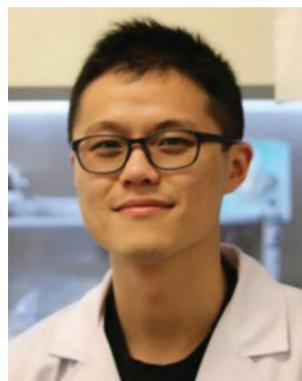
Shuang Xiao is an associate professor at Center for Advanced Material Diagnostic Technology and College of Engineering Physics, Shenzhen Technology University. He received his BS degree (2012) from the School of Physics, Huazhong University of Science and Technology and his PhD degree (2017) from the Department of Chemistry, the Hong Kong University of Science and Technology under the supervision of Prof. Shihe Yang.

Shuang Xiao

His current research is focused on compound semiconductors, X-ray detectors, and solar cells.

This journal is © The Royal Society of Chemistry and the Chinese Chemical Society 2023
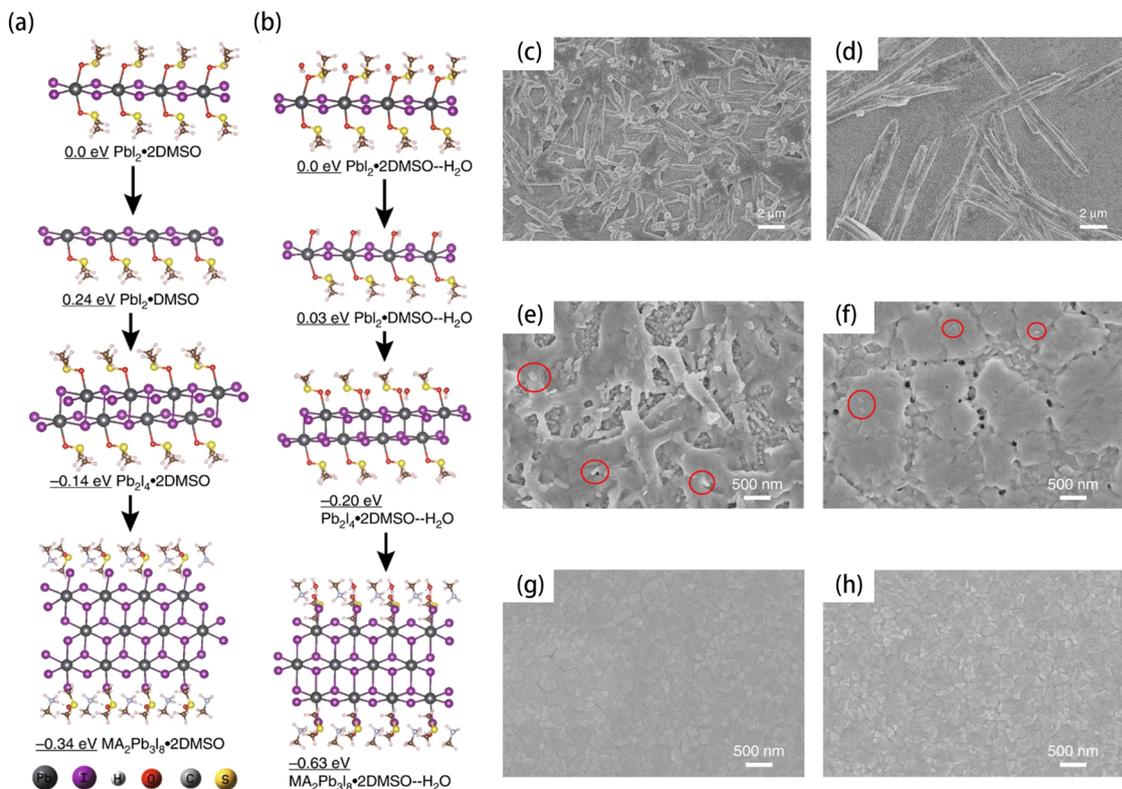
Fig. 1 Calculated structures and electronic energies of the lead complexes without H_2O (a) and with H_2O (b). The electron scanning microscopy (SEM) images of the $MA_2Pb_3I_8\cdot2DMSO$ intermediate made in (c) glove box and (d) ambient atmosphere without the antisolvent dripping step. The SEM images of (e) the intermediate films without annealing and (f) perovskite films after annealing at 98 °C for 7 min synthesized using the conventional method in ambient air. The SEM images of (g) the intermediate/perovskite films after aging, without annealing and (h) perovskite films after annealing at 98 °C for 7 min synthesized using the prenucleation method in ambient air. The scale bar is 2 μm in (c) and (d). The scale bar is 500 nm in (e)–(h). Reproduced from ref. 18 with permission from Springer Nature, copyright 2020.

are *N*,*N*-dimethylformamide (DMF) and dimethyl sulfoxide (DMSO). They can bind with Lewis-acid molecules such as lead iodide (PbI_2) to form the Lewis acid–base adduct such as $PbI_2\cdot$ DMSO, $MA_2Pb_3I_8\cdot2DMSO$, and $MA_2Pb_3I_6\cdot2DMF$.[18,43–45] These adducts are named as Lewis acid–base intermediates. To date, a great number of intermediates have been found, which depend on the type of binding forms. The chemical properties of intermediates could significantly influence the growth of the perovskite crystal.

The ambient water could accelerate the formation of lead-based intermediates, which is harmful and results in the uncontrolled growth of halide perovskites.[18] To uncover the mechanism related to the water-influenced formation of intermediates, Zhang *et al.* compared the conversion processes from the $PbI_2\cdot2DMSO$ complex to the $MA_2Pb_3I_8\cdot2DMSO$ intermediate in a glove box and in ambient air. As shown in Fig. 1(a) and (b), they calculated the electronic energy of each intermediate state. In the anhydrous environment, the electronic energy of $PbI_2\cdot$ DMSO and $PbI_2\cdot2DMSO$ was 0.24 eV and 0.0 eV, respectively. This implies the difficulty in eliminating DMSO from $PbI_2\cdot$ 2DMSO. Thus, the formation of $PbI_2\cdot DMSO$ and $MA_2Pb_3I_8\cdot$ 2DMSO is slow in an anhydrous environment. However, in ambient air, the H_2O molecule yields a low electronic energy of $PbI_2\cdot DMSO–H_2O$ (0.03 eV), which made it easier to remove

DMSO from $PbI_2\cdot2DMSO–H_2O$. Thereafter, the formation of $MA_2Pb_3I_8\cdot2DMSO$ should be accelerated with the help of ambient water.

As expected, the size of the $MA_2Pb_3I_8\cdot2DMSO$ intermediate grown in ambient air was significantly larger than those grown in a glovebox (Fig. 1(c) and (d)). Even employing antisolvent dripping in the fabrication process, the water-induced large fibrillar crystallites still existed (Fig. 1(e)). Thereafter, the quality of perovskite films could be poor because of the very large intermediate fibers. As shown in Fig. 1(f), the perovskite film converted from intermediates shown in Fig. 1(e) was rough and had many pinholes, whose morphology appeared as mixed nanosized blocks and rods. To address this issue, they developed a prenucleation strategy, which includes several times of dripping to advance the nucleation process and prevent the overgrowth of intermediates. The intermediate film fabricated by the prenucleation method was smooth and free of pinholes. Irrespective of without or with annealing, the intermediate could transfer into a high-quality perovskite film, which is shown in Fig. 1(g) and (h). The solar cells fabricated by the prenucleation method achieved an average PCE of 18.8% with a strikingly small standard deviation of 0.43%. Furthermore, the PVSCs showed impressive stability. After 100 days of storage in a dry N_2-filled glove box, the unencapsulated PVSCs only lost

about 10% of the initial efficiency. In addition, the prenucleation method is much more tolerant to the changes in environmental humidity and impurity of chemicals than that of conventional methods, which should be an advantage for large-scale fabrication in industry.

Yang *et al.* developed a low-dimensional intermediate-assisted growth (LDIAG) method to fabricate the $CsPbI_2Br$ film in ambient atmosphere.[46] In this method, they introduced imidazole halide (IMX) such as IMI and IMBr into the precursor. Fig. 2(a) showed the crystallization process of the LDIAG film. The IMX combined with the precursor's molecules to form the 2D $(IMCs)_2PbI_{4-x}Br_x$ intermediate instead of the unstable 3D perovskites. By introducing the 2D intermediate, this procedure could prevent the direct formation of unstable $CsPbI_2Br$ and retard the crystallization rate. To prove this, they stored the precursor films with and without IMX in ambient air (RH: 30%). The intermediate film with IMX was still yellow after 3 h storage in air, while the film without IMX turned to brown in 2 min (Fig. 2(b)). After annealing, the control perovskite film made with IMX-free precursors was rough, full of pinholes, and had small grains with a thickness of 370 nm (Fig. 2(c)). In stark contrast, the perovskite film fabricated by the LDIAG method was compact, smooth, had no pinholes, and had large grains with a thickness of 560 nm, indicating a significantly improved film quality. The PVSCs fabricated by the LDIAG method showed a maximum PCE of 17.26%, which is remarkably larger than the control PVSCs fabricated in air (PCE: 9.10%) and glove box (PCE: 15.67%).

In a similar way, Budiawan *et al.* added core-twisted tetrachloroperylene diimide (ClPDI) derivatives (n-type small molecules) into precursor solutions and used two-step method to deposit the $MAPbI_3$ film. The ClPDI molecules have carbonyl (C=O) groups, which could act as Lewis base and combine with Pb^{2+} ions to form Lewis adducts.[47] The formation of Lewis adducts could passivate the Lewis acid traps from uncoordinated Pb^{2+} ions and lower crystallization rate of the perovskite

films to improve the crystallinity. Benefiting from the above effects, the perovskite films with CIPDA exhibited higher steady-state photoluminescence (PL) than that of the control perovskite films, which indicated that the nonradiative recombination was reduced by CIPDA. The PVSCs with CIPDA achieved a champion PCE of 18.77%, which is higher than the PCE of the control PVSC (PCE = 15.88%). For the device stability, the modified PVSCs maintained 90% of its PCE after 720 h storage inside a glove box.

Li *et al.* added 2-hexyl-thiophene (2HT) into the precursor solutions and used the antisolvent dripping method to fabricate the $MAPbI_3$ film.[48] 2HT could combine with PbI_2 molecule to form the intermediate in the precursor solution. This kind of organic group-anchored intermediates could increase the activation energy of nucleation to prevent the formation of additional nuclei as well as accelerate the growth of perovskites (Fig. 3(a)). Thus, the perovskite film with 2HT showed larger grain sizes and more uniform surface than the control film (Fig. 3(b)). Besides, time-resolved photoluminescence (TRPL) curves showed that the decay time of 2HT-modified perovskite films is significantly larger than that of the control perovskite films. This indicates that the nonradiative recombination was suppressed in the perovskite films with 2HT. As the major nonradiative sites are defects, the TRPL results also implies that 2HT could reduce the defects density of perovskites, which agrees well with the morphology change. With the assistance of 2HT, the modified PVSCs reached a PCE of 20.61%, which is higher than that of the pristine PVSCs (PCE = 18.65%).

The fast volatilization of DMF could facilitate the homogenous nucleation of quasi 2D perovskite $[(BA)_2(MA)_3Pb_4I_{13}]$ and thus resulted in random-orientated perovskite grains.[49] As a consequence, many unfavorable cracks and pinholes formed on the surface of perovskite films. To solve this problem, Zhang *et al.* developed a binary solvent engineering of DMF/DMSO in the precursor solution. In this method, DMSO was coordinated with the solute molecules to form the intermediate
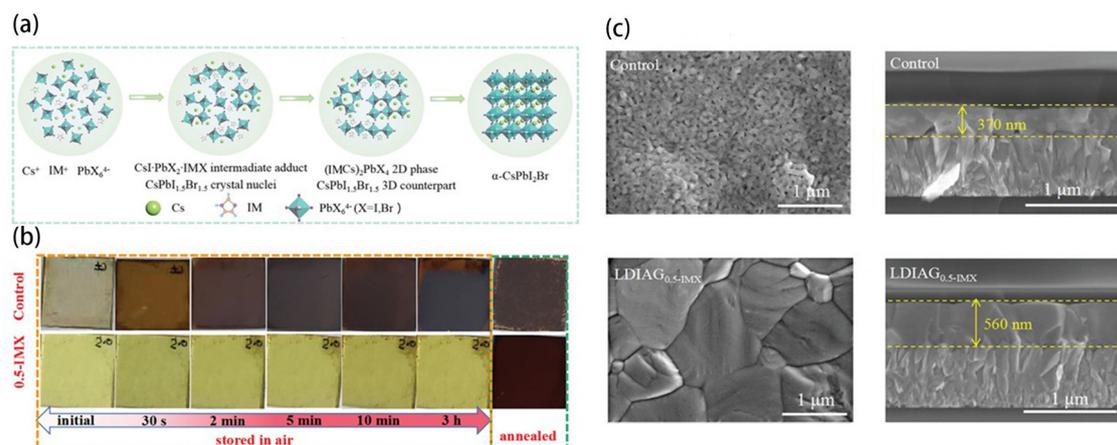

Fig. 2 (a) The crystallization process of low-dimensional intermediate-assisted growth of halide perovskites film with an imidazole halide ($LDIAG_{0.5-IMX}$). (b) Optical photographs of the two perovskite precursor films (control and $LDIAG_{0.5-IMX}$) stored in ambient air for different times (yellow dashed box) and annealed at 240 °C after 3 h storage (green dashed box). (c) The top-view and cross-section SEM images of the control perovskite film and the $LDIAG_{0.5-IMX}$ film. The scale bar is 1 μm. Reproduced from ref. 46 with permission from Wiley-VCH, copyright 2021.
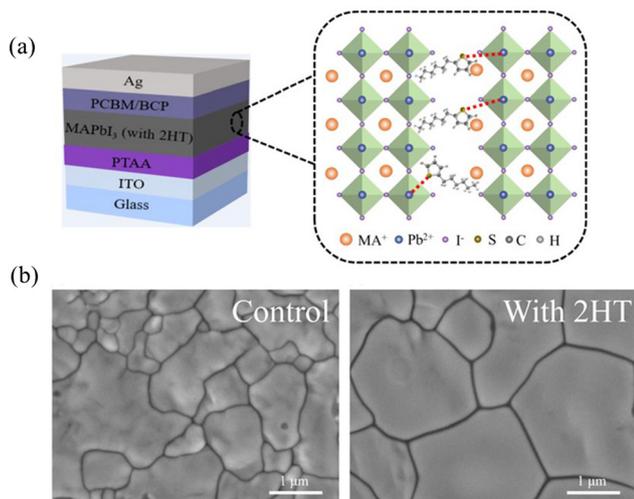
Fig. 3 (a) Schematic illustration of the mechanism of 2-hexyl-thiophene (2HT) passivation for perovskite films. (b) Top-view SEM images of the control and 2HT-modified perovskite films. The scale bar is 1 μm. Reproduced from ref. 48 with permission from Wiley-VCH, copyright 2022.

of benzylamine hydroiodide (BAI)/methylammonium iodide (MAI)/PbI_2/DMSO. The formation of this intermediate could slow the crystallization process, which enabled the growth of high-quality perovskite films.

The fast crystallization of wide-bandgap perovskite, $Cs_{0.17}FA_{0.83}PbI_{1.8}Br_{1.2}$, could lead to high trap density and hinder the further enhancement of PV performance. To address this issue, Yu et al. introduced a FACl additive in the precursor solution.[50] With the addition of FACl, a stable and phase-pure intermediate thin film, $Cs_{0.17}FA_{1.83}PbI_{1.8}Br_{1.2}Cl$, was formed. This phase-pure intermediate could lower the crystallization rate of perovskites and allow the obtained perovskite films to have favorable morphology such as brighter appearance, larger crystal grain sizes, and smooth surface than those of pristine films. Compared with the pristine films, the perovskite films converted from $Cs_{0.17}FA_{1.83}PbI_{1.8}Br_{1.2}Cl$ exhibited higher quantum efficiency and lower trap density, which is based on the PL mapping results. The PVSCs based on modified perovskites showed higher PCE of 19.02% than the PCE (15.07%) of PVSCs based on pristine perovskites, which was fabricated by the conventional method.

The intermediate also plays an important role in the growth of a mixed perovskite. During the formation of a mixed-perovskite, $FA_{1-x}MA_xPbI_3$, the crystalline phase of intermediate films, could influence the resulting perovskite film's morphology, crystallinity and electronic property.[51] In the experiment, the intermediate film prepared in ambient air was a δ nonperovskite phase of $FA_{1-x}MA_xPbI_3$. But the control intermediate film prepared in N_2 glove box was an α-perovskite phase of $FA_{1-x}MA_xPbI_3$. The perovskite films, which converted from the δ-phase intermediates, showed larger grain sizes, less densities, higher crystallinity, and better stability than those of the perovskite films converted from α-phase intermediates. Moreover, the perovskite films converted from δ-phase intermediates

had less nonrecombination losses, higher absorbance, and longer carrier life time, compared with ones from α-phase intermediates. The PVSCs based on δ-phase intermediates showed a champion PCE of 22.09%, while the control device only showed a PCE of 20.38%.

In ambient air, the α-phase $FAPbI_3$ (α-$FAPbI_3$) perovskite is easy to convert to δ-phase $FAPbI_3$ (δ-$FAPbI_3$). To fabricate stable α-$FAPbI_3$ perovskite in ambient air, Wang et al. developed a solution-based method, which employed the N-methyl pyrrolidone (NMP) additive.[52] The NMP could combine with formamidinium iodide (FAI) and PbI_2 to form the FAI·PbI_2·NMP adduct without δ-$FAPbI_3$, while the precursor with DMSO additive yielded intermediates with δ-$FAPbI_3$. During the annealing process of intermediates, the detachment of NMP from FAI·PbI_2·NMP triggered the formation of α-$FAPbI_3$, which yielded high-quality perovskite films with a smooth and dense morphology. However, other intermediates experienced the transition from δ-$FAPbI_3$ to α-$FAPbI_3$, which could only produce less performed perovskite films compared with the FAI·PbI_2·NMP case. Through this route, a champion PCE of 17.29% was achieved, which was 10% higher than that of PVSCs fabricated without additives and 20% higher than that of PVSCs fabricated with DMSO.

In another work, Wang et al. reported an amorphous intermediate formed by the reaction between cesium iodide (CsI) and PbI_2.[53] The interaction between CsI and PbI_2 could convert the crystalline PbI_2 to a noncrystallized form, which produced the amorphous intermediate. This intermediate could improve the quality of perovskite films and was used to fabricated oriented perovskite films under ambient air condition. Using this method, the crystallinity of perovskite films was improved, and the grain size was improved from 0.46 μm to 0.96 μm. Corresponding to the improvement of the film morphology, the defect was suppressed and the nonradiative recombination reduced. The PVSCs based on this method achieved a champion PCE of 23.46%, which was larger than that of PVSCs fabricated in a glovebox (22.31%).

Because perovskite is sensitive to water and the outside atmosphere, although there have been more studies on improving the resistance of perovskite to water and the outside atmosphere, a considerable part of the perovskite film of high-performance perovskite batteries is still grown in non-atmospheric environments. Some recent advances in perovskites manufactured in non-atmospheric environments are described below.

To produce high-quality $FAPbI_3$-based PVSCs, Ge et al. develop an effective method called 2,2-azodi(2-methylbutyronitrile) (AMBN) intermediate phase engineering (AMBN-IPE) to solve incomplete and random transformation of PbI_2 films with organic salts by introducing AMBN into the precursor solution.[54] The AMBN has two symmetrical cyano groups (C≡N) that contain lone-pair electrons from N, which can coordinate with the PbI_2 to form the AMBN–PbI_2 intermediate. This intermediate could induce the aggregation of the precursor solution to form mesoporous PbI_2 films, which is beneficial for the complete reaction between PbI_2 and organic precursor

and the formation of α-FAPbI$_3$. At the same time, the AMBN also could react with FAI to form the FAI–AMBN intermediate, which could suppress the vigorous reactivity of FA$^+$ ions and lead to the ordered reaction between PbI$_2$ and organic precursors. Therefore, the perovskite films produced by AMBN-IPE showed less defect density and more stable structure than the control films because the above reaction also passivated the uncoordinated Pb^{2+} and FA$^+$ and released the residual strain. The FA$_x$MA$_{1-x}$PbI$_3$-based PVSCs fabricated by AMBN-IPE achieved a champion PCE over 25% and a stabilized PCE of 24.8%. Furthermore, the device retained 96% of its initial PCE under 1000 h continuous white light illumination with an intensity of 100 mW cm^{-2} at ≈ 55 °C in N$_2$ atmosphere.

Li et al. reported a hydrogen bond-bridged intermediate (GBAC–PbI$_2$–DMF) by adding a multifunctional molecule (4-guanidinobenzoic acid hydrochloride (GBAC)).[55] This intermediate could slow down the crystallization rate and control the nucleation rate, which can improve the crystallinity and stability of perovskite films. The inverted PVSCs fabricated by this method achieved a champion PCE of 24.8% with an open-circuit voltage (V_{oc}) of 1.19 V, short-circuit current density (J_{sc}) of 24.55 mA cm^{-2}, and fill factor (FF) of 84.78%. Furthermore, the device showed T98 lifetime over 1000 h under continuous heating at 65 $\pm$ 5 °C in a nitrogen-filled glovebox.

Moreover, McMeekin et al. developed a high-temperature dimethyl sulfoxide-free method that utilized dimethylammonium halide (DMAX) to control the intermediate phases and adjust the crystallization process.[56] The DMAX could induce the formation of hexagonal perovskite polytype (2H, 4H, and 6H) intermediate phases, which can decrease the crystallization speed. In this way, the crystallization kinetics of FA$_y$Cs$_{1-y}$Pb(I$_x$Br$_{1-x}$)$_3$ perovskites could be controlled to realize the growth of the highly ordered face-up domains. The perovskite films after adding DMAX showed larger grain sizes, higher crystallinity, and more compact surface than the pristine films. The PVSCs fabricated by this method achieved a champion PCE of 20.2%, while the control PVSCs showed 18.8%. Furthermore, the DMAX PVSCs showed a T80 (the time over which the device PCE decreases to 80% of its initial value) lifetime of 1410 (1190) h for the champion (median) PVSCs, while the control DMF/DMSO device showed 1040 (780) h for the champion (median) device.

For the low-dimension perovskite, Wang et al. developed an intermediate engineering method for quasi-2D Ruddlesden–Popper (RP) perovskites, (BDA)(MA)$_4$Pb$_5$I$_{16}$, by introducing the sulfonium cations into the precursor solution.[57] In the control precursor solution without sulfonium cation, it is easy for the PbI$_2$ and MAI to react with DMF/DMSO to form [(MA$^+$)$_2$-(PbI$_3$)$_2$·S$_2$] (S = DMSO/DMF) and (PbI$_2$)$_2$·S$_2$ intermediates. The (MA$^+$)$_2$(PbI$_3$)$_2$·S$_2$ can easily transform to the perovskite fiber (MAPbI$_3$) by losing the solvent. But the (PbI$_2$)$_2$·S$_2$ could convert to (MA$^+$)$_2$(PbI$_3$)$_2$·S$_2$ by adding ammonium salts and could also turn back to PbI$_2$ by losing the solvent. The two transformation processes could be uncontrollable and resulted in disordered crystallization, which is harmful for perovskites. The sulfonium cations could induce the formation of (MA$^+$)$_2$(PbI$_3$)$_2$·S$_2$ and

inhibit the formation of (PbI$_2$)$_2$·S$_2$, which led to the ordered crystallization of (BDA)(MA)$_4$Pb$_5$I$_{16}$. The PVSCs fabricated by this method showed a champion PCE of 19.08% at room temperature and 20.52% at 180 K with decent stability. In another work, Xu et al. produced 2D Cs$_2$PbI$_2$(SCN)$_2$ by adding FACl into the precursor solution, which could induce the formation of the Cs$_2$PbI$_{2-x}$Cl$_x$(SCN)$_2$ intermediate.[58] This intermediate could slow down the crystallization rate and passivate the I$^-$ vacancies. The perovskite films with FACl showed less defect density and larger grain sizes than the pristine ones. The PVSCs fabricated by this method showed a champion PCE of 4.7%.

Moreover, Yang et al. developed a dual-component green solvent consisting of isopropyl acetate (IA) and acetonitrile (ACN) for MAPbI$_3$ perovskite fabrication.[59] The IA and ACN could slow down the nucleation rate and assist the formation of room temperature-stable perovskite intermediate phase, CH$_3$NH$_3$I·PbI$_2$·CH$_3$NH$_2$ (MAI·PbI$_2$·MA), which could convert to the perovskite by simple thermal annealing. In addition, the released MA gas could passivate the defects during the annealing process. Therefore, the final perovskite showed better film morphology and PV performance than the control ones. The PVSCs reached PCEs of 20.80% and 16.37% for the areas of 0.04 cm^2 and 14.08 cm^2, respectively.

To promote the complete transformation from the intermediate to perovskite, Tang et al. developed a highly efficient phase-transition pathway using a polydimethylsiloxane (PDMS)-based facial mask incubation technique, which could slow down the perovskite crystallization rate and depress the perovskite aggregation behavior.[60] They fabricated inverted PVSCs with a champion PCE of 20.93% and high stability, whose PCE was maintained at 91% of the initial value after shelf storage over 3700 h in an inert atmosphere and 80% of the initial value after 1190 h under continuous one sun illumination.

In this section, we discussed the typical methods of using intermediates to control the crystallization reactions of perovskites. The rational usage of intermediates can control the crystallization rate of perovskites, inhibit undesirable nucleation, improve the quality of films, and finally increase the performance of PVSCs.

2.2 Reaction conditions

The reaction conditions can significantly influence the formation of perovskite films.[61–68] The perfect control of the reaction conditions can greatly improve the quality of the perovskite. In this section, three reaction conditions of temperature, pressure, and concentration as well as their effects on the perovskite will be discussed. At the same time, we will show several methods to improve the quality of the perovskite by controlling these reaction conditions.

2.2.1 Temperature. Ren et al. changed the temperature of the ammonium salt precursor solution to fabricate (FAPbI$_3$)$_{1-x}$-(MAPbBr$_3$)$_x$, FA$_x$MA$_{1-x}$PbI$_3$, and MAPbI$_3$ with two-step methods.[69] They found that all the perovskite films' grain sizes were enlarged with the increase in the temperature of ammonium salt

5314 | Mater. Chem. Front., 2023, **7**, 5309–5332

This journal is © The Royal Society of Chemistry and the Chinese Chemical Society 2023

precursors. In addition, the grain sizes of perovskite films with different composition followed the sequence of $(FAPbI_3)_{1-x}$-$(MAPbBr_3)_x$ > $FA_xMA_{1-x}PbI_3$ > $MAPbI_3$ under the same fabrication temperature. This result indicates that adding FA or Br into the precursor will make the grain sizes even larger. Intuitively, the larger grain sizes of halide perovskite films imply less defects and thus higher performance of the PVSCs. But enlarged grains with increasing temperature was not monotonously positively related to the improved performance of PVSCs. A very-high reaction temperature can cause the formation of photovoltaic nonactive phase and deteriorate the performance of PVSCs. The rivalry between the two effects of the high reaction temperature decides that the optimized temperature for fabricating $(FAPbI_3)_{1-x}(MAPbBr_3)_x$, $FA_xMA_{1-x}PbI_3$, and $MAPbI_3$-based PVSCs were 30 °C, 30 °C, and 55 °C, respectively.

Kim *et al.* also observed the high temperature-induced degradation of halide perovskites.[70] To avoid this, they chose to shorten the annealing time. Their annealing conditions are: (a) 100 °C for 30 min (HTSA-100), (b) 200 °C for 2 min (HTSA-200), (c) 300 °C for 8 s (HTSA-300), and (d) 400 °C for 4 s (HTSA-400). The grain sizes of HTSA-100, HTSA-200, HTSA-300, and HTSA-400 are 300 nm, 500 nm, 700 nm, and 1 μm, respectively. Besides, perovskites merely suffered decomposition under such annealing conditions. As a result, the PVSCs made with HTSA-400 showed a PCE of 20.75%, which was the best among the four conditions.

For the slot die-coating–based PVSCs, the temperature is also an important parameter, which significantly influences the growth of perovskite films.[71] The grain size and crystallinity of perovskite films increased as the temperature of the substrates increased from 70 °C to 130 °C. However, they decreased when the temperature further increased from 130 °C to 150 °C. Corresponding to the change in the surface morphology and crystallinity, PVSCs reached the highest PCE of 15.40% at 130 °C among all the conditions.

2.2.2 Concentration. Modulating the concentration of precursors is an effective way to control the quality of perovskite films.[72] Du *et al.* investigated the impact of precursor concentration on $Cs_{0.05}FA_{0.8}MA_{0.15}Pb(I_{0.84}Br_{0.16})_3$ perovskite crystallization. In Fig. 4(a) and (b), the top-view SEM images and curve of film thickness showed that the grain size and thickness of perovskite films increased with the increase in the precursor concentration from 0.8 M to 2.3 M. The perovskite films made with 2.3 M precursors (2.3 M-PVK) exhibited the largest thickness and grain size among all the conditions, which proved that the increasing concentration could be beneficial to crystal growth. Furthermore, they characterized the absorption of perovskite films from 550 nm to 850 nm and found that the absorption of perovskite films increased as their thickness increased (Fig. 4(c)). The 2.3 M-PVK exhibited the highest absorption among all precursor concentrations. However, according to the PL spectra result, the perovskite films with the 2.0 M precursor exhibits the highest PL intensity while the perovskite films with 2.3 M precursor showed the lowest PL intensity, which indicated that the perovskite films

made with the 2.0 M precursor had lower trap density than that of the perovskite films made with the 2.3 M precursor. Therefore, they obtained the champion PCE of 21.13% of PSCs with a 2.0 M precursor concentration.

Du *et al.* developed a two-step sequential deposition method to fabricated hole-transport-layer-free carbon-based $MAPbBr_3$ PVSCs.[73] In their work, they firstly spin-coated the precursor solution ($PbBr_2$ and MABr) on the substrate. Then, the additional MABr solution was dropped into the precursor solution to slightly increase the concentration of MABr. The increase in the MABr concentration could promote the dissolution of $PbBr_2$ and the transition from $PbBr_2$ to $MAPbBr_3$. Therefore, perovskite films fabricated by this method exhibited better crystallinity, lower trap density, and longer carrier lifetime. The PVSCs showed forward scanning PCE of 6.88% and reverse scanning PCE of 7.64%, and no significant PCE degradation was observed after the PVSCs was stored in dry air for one year.

2.2.3 Pressure. Similar to temperature, pressure is also a key parameter in the process of perovskites' growth, which has an obvious impact on their morphology, defects, carrier mobility, *etc.*[74] Luo *et al.* investigated the impact of pressure on the perovskite films and developed a pressure-assisted solution processing (PASP) method to improve the quality of perovskite films.[75] The procedure of the PASP method is depicted in Fig. 5(a). They firstly spin-coated the precursor solution on top of a TiO_2 film. Two perovskite precursor films were then placed face-to-face and different pressures were applied. After that, they were annealed at 110 °C for 60 min to convert into perovskite films. As the pressure increased from 1225 to 12 250 Pa, the grain sizes of perovskite films were remarkably enlarged from several hundred nanometer to ∼3 μm (Fig. 5(b)). Nonetheless, when the pressure increased from 7350 Pa to 12 250 Pa, several cracks appeared on the grains. According to the result, the pressure of 4900 Pa was selected in further studies. In particular, they analyzed the extrinsic moisture-induced degradation of PVSCs by synchrotron-based two-dimensional grazing incidence X-ray diffraction (2D-GIXD) to study the influence of PASP on the stability of PVSCs. For the control film without the PASP method, its decomposition was evidenced by the appearance of hydrated perovskites and excessive PbI_2. On the contrary, no hydrated pattern could be observed for PVSCs with the PASP method, indicating negligible degradation. These results indicated that the large grain sizes of PASP-perovskites could effectively improve their stability when facing moisture. Besides, the PCE of PVSCs with the PASP method was 20.74%, which was higher than the PCE of control PVSCs (18.11%).

In this section, we introduced methods to improve the quality of perovskite films by controlling the reaction conditions: (1) reaction temperature engineering, (2) concentration engineering, (3) pressure engineering. By adjusting the temperature, we can significantly improve the surface morphology of the perovskite film, reduce the concentration of the defect state, and finally improve the performance of perovskite films. By adjusting the concentration and proportion of one or several solutes, the solubility of some solutes can be improved, the
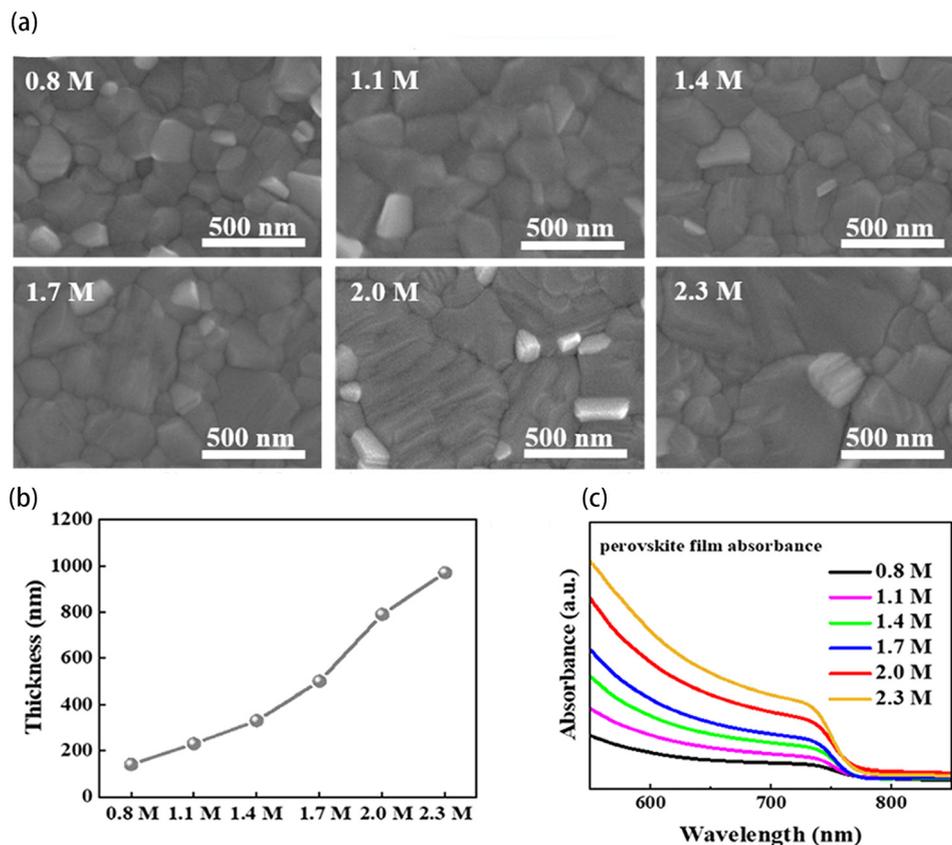
Fig. 4 (a) SEM images of the perovskite films with various precursor concentrations. The scale bar is 500 nm. (b) Thickness of perovskite films and (c) absorption spectra of perovskite films with various precursor concentrations. Reproduced from ref. 72 with permission from Multidisciplinary Digital Publishing Institute, copyright 2022.

surface morphology of the perovskite can be improved, and the defects can be reduced. Regulating the pressure in the process of perovskite film growth can make the perovskite film more compact and enlarge the grains. However, due to the poor mechanical properties of the perovskite, excessive pressure will destroy the perovskite film. Notably, the success of these methods is based on the precise control of the reaction conditions, but even a deviation from the reaction conditions can damage the morphology and performance of perovskite.

3. Additive-controlled growth

In recent years, additives have been widely utilized to control the crystallization process and improve the quality of various perovskites.[76–79] Besides, great number of additives has been developed, encompassing both inorganic substances and organic compounds. The functional groups or specific ions of these additives could influence the formation reaction of perovskites in precursors. In this way, we can regulate the crystallization rate of the perovskite through the usage of specific additives and eliminate some impurity phases in the crystallization process. Furthermore, the additives can effectively control the surface morphology and internal defects of the perovskites as well as improve the photoelectric properties

and stability of perovskite films.[80–82] In this section, several typical additives will be introduced, which are divided into two parts: (1) organic additives and (2) inorganic additives.

3.1 Organic additives

Polymers have been widely blended into precursors to improve the quality of perovskite films. Ning et al. blended a biodegradable polymer macromolecule, poly(D,L-lactide) (PDLLA) into precursor solutions, to fabricate MAPbI$_3$ films with good crystallinity.[83] The Fourier transform infrared (FTIR) spectra show that the C=O groups and O–H groups stretching vibration in perovskite films containing PDLLA were at about 1738 and 3457 cm^{-1}, respectively (Fig. 6(a)). These peaks could confirm the strong molecular chemical interaction between PDLLA and the perovskite. Moreover, the X-ray photoelectron spectroscopy (XPS) shows that the pristine perovskite had Pb^{2+} peaks at 138.2 and 143.1 eV, and the metallic Pb peaks were located at 136.4 and 141.3 eV (Fig. 6(b)). After blending PDLLA, the peaks of Pb^{2+} shifted to lower binding and the metallic peaks disappeared, which indicated the electron donation of the C=O functional groups of PDLLA to Pb^{2+} ions. The interaction between PDLLA and the perovskite precursor decreased the free energy of crystallization and prompted the formation of larger grain sizes. Compared to the film without PDLLA,
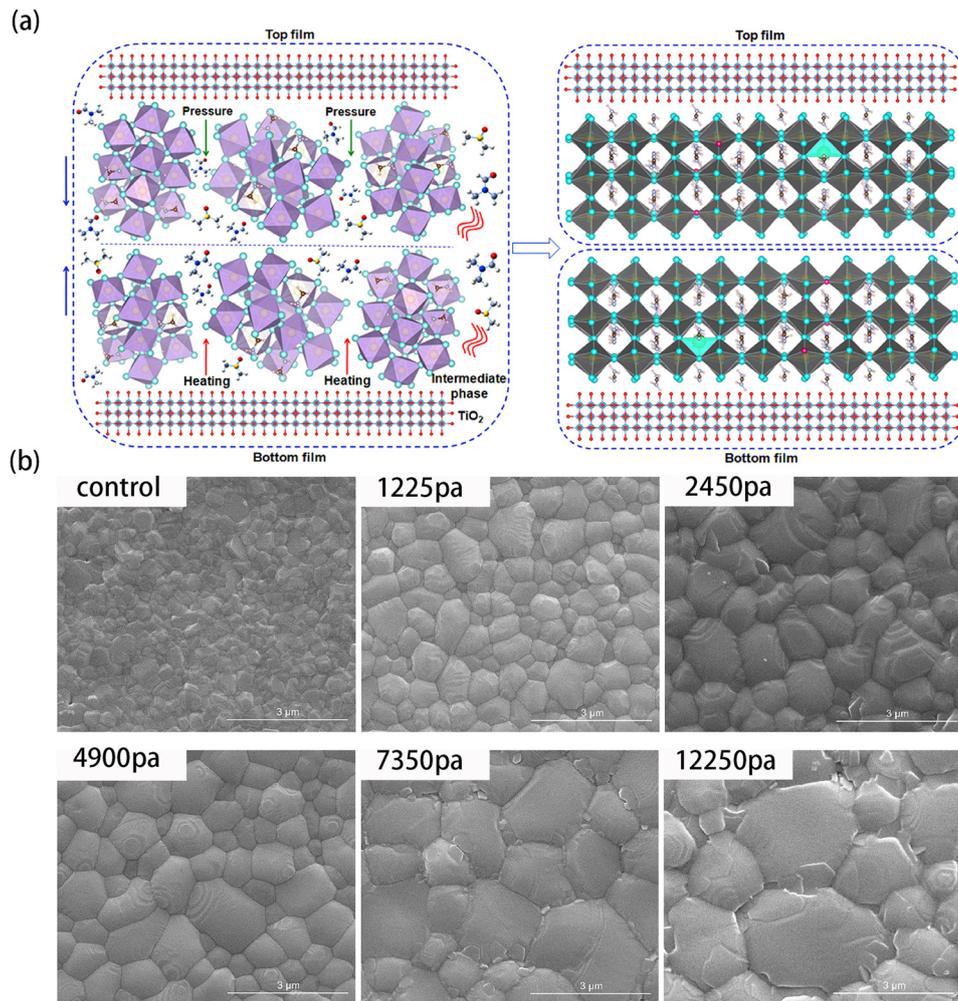
Fig. 5 (a) Schematic of the fabrication procedure of perovskite films using pressure-assisted solution processing (PASP). (b) Top-view SEM images of the control and PASP perovskite films with a pressure of 1225, 2450, 4900, 7350, and 12 250 Pa. The scale bar is 3.0 μm. Reproduced from ref. 75 with permission from Elsevier, copyright 2020.

the average grain sizes of the film with PDLLA were significantly enlarged (Fig. 6(c) and (d)). With the addition of PDLLA, the PDLLA-integrated PVSCs achieved a champion PCE of 18.94% on the rigid substrate and 16.61% on the flexible substrate. The control device only showed a PCE of 13.38% on the flexible substrate.

Polymers could also be blended into inorganic perovskites. Zhang *et al.* introduced polyethylene glycol (PEG) into the precursor solution to modify the $CsPbI_2Br$ films.[84] The SEM images of $CsPbI_2Br$ films with different concentrations of PEG are shown in Fig. 6(e). The control perovskite film without PEG exhibited a rough surface with uneven grain sizes and indistinct boundary. On the contrary, the film with the addition of 0.25 mg PEG showed compact and uniform grains, which should be beneficial to the PV performance. However, when 0.5 mg or 1.0 mg PEG was added, the films showed smaller grain sizes than those of films with 0.25 mg PEG. Furthermore, there were some gaps between the grains, which could lead to current leakage and are harmful for PVSCs. The reason for this may be because the oxygen atoms of PEG interacted with lead

ions to accelerate the nucleation rate, which could decrease the grain sizes. The PCE of modified PVSCs with PEG improved from 10.09% to 13.59%. Furthermore, the modified PVSCs with PEG not only had lower trap density of 8.35×10^{16} cm^{-3} than that of the control PVSCs (9.57×10^{16} cm^{-3}) but also had lower dark current than that of the control PVSCs.

In addition to the examples mentioned above, there are many kinds of polymeric additives that could improve the quality of perovskite films, such as polyvinylpyrrolidone (PVP), polyamidoamine (PAMAM), poly(vinylidene fluoride-*co*-hexafluoropropylene) (PVDF-HFP), poly(vinylidene fluoride-*co*-trifluoroethylene) P(VDF-TrFE), polymethyl methacrylate (PMMA), and mixture of polymers. Zhong *et al.* added a mixture of PVP and PEG into perovskite precursors.[85] C=O groups in PVP have strong interaction with Pb^{2+} and O atoms in PEG, which have intense hydrogen bond with H atoms in $CH_3NH_3^+$. This interaction between the polymer mixture and perovskite could adjust the position of the crystal nuclei to make them evenly distributed in PVP chains, which was beneficial to the homogeneous nucleation and the formation of dense perovskite
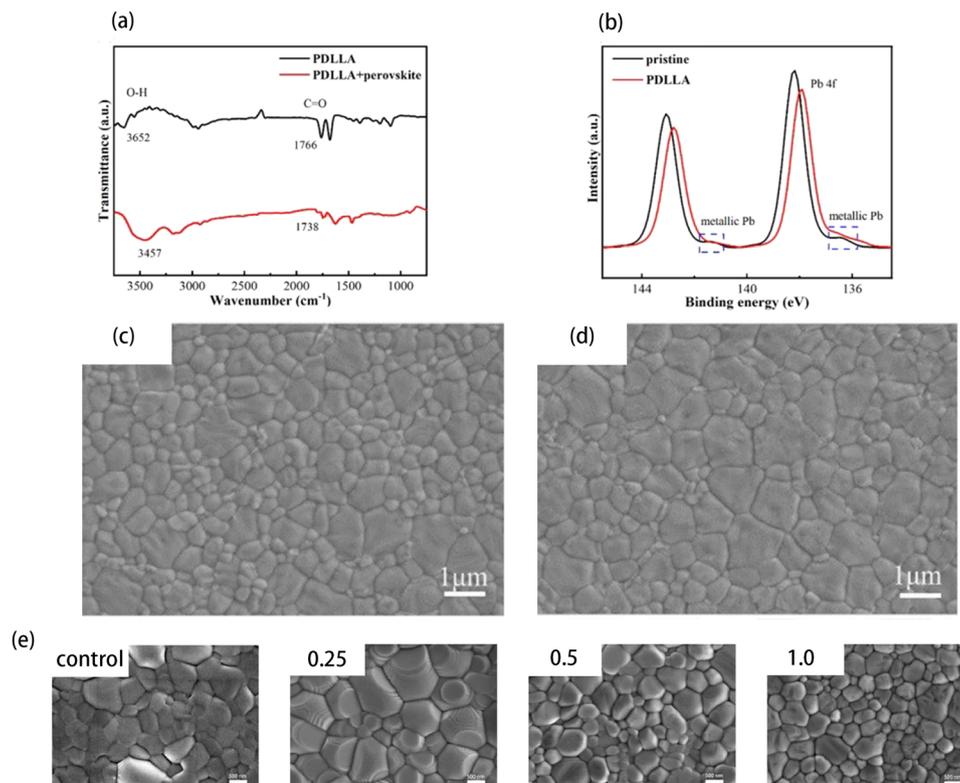
Fig. 6 (a) Fourier transform infrared spectroscopy (FTIR) spectra of polymer and cross-linked perovskite film. (b) X-ray photoelectron spectroscopy (XPS) of the Pb 4f orbital of $MAPbI_3$ without and with polymer integration. The SEM images of (c) pristine and (d) optimized films. The scale bar is 1.0 μm. Reproduced from ref. 83 with permission from Springer Nature, copyright 2022. (e) SEM images of $CsPbI_2Br$ films modified with different PEG concentrations: control, 0.25 mg mL^{-1}, 0.5 mg mL^{-1}, 1.0 mg mL^{-1}. The scale bar is 500 nm. Reproduced from ref. 84 with permission from Elsevier, copyright 2021.

films. In this way, they successfully controlled the crystallization process of the perovskite film and eventually improved the PCE of PVSCs from 7.71% to 9.63%. Shaik *et al.* used PAMAM as an additive to prepare the precursors.[86] The amine functional groups of PAMAM could chelate with Pb^{2+} in the precursor solution and inhibit the nucleation and growth of the perovskite along the (110) direction, which influenced the crystallization kinetics of the $MAPbI_3$ perovskite. Narendhiran *et al.* reported a method of using PVDF-HFP as an additive.[87] The high electronegative fluorine atoms in PVDF-HFP could combine with hydrogen atoms of the MA cation and form hydrogen bonds, which could reduce the nucleation rate during the crystallization process of the perovskite. In this way, the perovskite films showed enlarged grain sizes and improved crystallinity. Furthermore, the hydrogen bond could prevent the degradation of PVSCs from moisture. To obtain compact and smooth perovskite films, Wu *et al.* added various polymer additives to the 10.0 mol% Ba-doped mixed-cation perovskite.[88] With the addition of P(VDF-TrFE) and PMMA additives, the pinholes of perovskite films were reduced. However, P(VDF-TrFE) and PMMA precipitated on the films' surface, which was an obstacle for charge transportation. In stark contrast, the perovskite films with PEG showed no pinholes and precipitates as PEG has better solubility in perovskite precursors than that of P(VDF-TrFE) and PMMA. He *et al.* blended $\sim$3 wt% PVP into a perovskite

precursor containing $\sim$30 vol% water to improve the quality of $MAPbI_3$ films.[89] With a hot-casting strategy, perovskite films with PVP showed a (200) plane-oriented growth and compact morphology. However, perovskite films without PVP showed a (110) plane-oriented growth and uneven morphology.

Small molecules could also be used as additives. Zhao *et al.* used (benzylamine)trifuoroboron (BBF) as an additive to improve the quality of the $FAMAPbI_3$ perovskite.[90] The FA/MA ions of MAI and FAI could combine with the fluorine atoms of BBF to form hydrogen bonds (N–H⋯F) in the precursor solution. Besides, the fluorine atom and N–H groups could combine Pb ions and I ions to from ionic bond. Therefore, the BBF can passivate cationic and anionic perovskite defects. The perovskite films with BBF showed lower trap density of 5.87 × 10^{15} cm^{-3} and higher carrier average lifetime of 676.66 ns than those of the control films (trap density = 8.67 × 10^{15} cm^{-3}, carrier lifetime = 242.63 ns). Furthermore, the PVSCs with BBF exhibited higher PV performance than the control PVSCs; the PVSCs with BBF achieved J_{sc} of 25.33 mA cm^{-2}, V_{oc} of 1.14 V, FF of 0.81, and PCE of 23.24%, while the control PVSCs only showed a PCE of 21.6%.

The RbCsFAMA-based multication perovskites show great potential for PVSCs because of their narrow bandgap and high lattice stability. Wang *et al.* introduced an aromatic zwitterion, 1-(3-sulfopropyl)pyridinium hydroxide inner salt (SPHI), into

the perovskite precursor.[91] The sulfonic group could interact with the Pb^{2+} and passivate the under-coordinated Pb^{2+} defect. Also, the pyridine N$^+$ of SHPI could have the electrostatic interaction with the I$^-$ and compensate the FA vacancy. Through the above interaction between SHPI and the perovskite, the quality of RbCsFAMA-based multication perovskite films has been greatly improved. Finally, the PCE of PVSCs, which used SHPI additive, was greatly improved to 25.01% (certified 24.60%).

3.2 Inorganic additives

Halides additive has played an important role in improving the quality of perovskite films. Park *et al.* developed an antisolvent dripping method, which used the alkylammonium chlorides (RACl) to control the crystallization process and improve the quality of α-FAPbI$_3$ perovskite films.[32] The RACl could bind to PbI$_2$ to form RA···H$^+$–Cl and lead to the deprotonation of RA$^+$, which resulted in the fast volatilization of RACl. Therefore, the type and amount of RACl could influence the δ- to α-phase transition rate, crystallinity, preferred orientation, and surface morphology of the final α-FAPbI$_3$. As shown in Fig. 7(a), the perovskite film with the FAPbI$_3$-containing 35 mol% methyl-ammonium chloride (MACl) (PA = 0) showed obvious grain boundaries and some pinholes. But with the addition of propylammonium chloride (PACl), the grain boundaries and pinholes disappeared, and the films were dense and uniform (PA = 5, 10, and 15). The result indicated that the increase in

RACl could decelerate the nucleation rate of the intermediate. They also investigated the surface morphology of perovskite films after annealing at 120 °C for 40 min, as shown in Fig. 7(b). All the films had dense and uniform surface, but the films with PACl showed an extremely flat surface. Then, they set the sample with 35 mol% MACl in the FAPbI$_3$ precursor solution, which is referred to as 'control', the sample with the addition of 10 mol% MACl and BACl is 'ref. 1 and 2', and the sample with the addition of 10 mol% PACl is the 'target'. The target had the highest PL intensity among all the samples according to the PL spectra (Fig. 7(c)). Furthermore, the TRPL spectra (Fig. 7(d)) showed that the target had the highest carrier lifetime of τ = 2929 ns, which was higher than that of the control and ref. 1 and 2 films (τ = 2187, 2582, and 1503 ns, respectively). The PL spectra and TRPL spectra indicated the lowest trap density in the target film, which led to the lowest nonradiative recombination among all the samples. For the PVSCs performance, the target achieved the J_{sc}, V_{oc}, FF values, and PCE of 25.69 mA cm^{-2}, 1.178 V, 86.15%, and 25.73%, respectively.

In another report in 2021, Zhang *et al.* used *n*-propyl-ammonium chloride (*n*-PACl) instead of MACl to fabricate FAPbI$_3$ PVSCs with high efficiency and stability.[92] The PA$^+$ cation in *n*-PACl could passivate the grain boundary of the FAPbI$_3$ films but could not be incorporated into the perovskite lattice due to the large ionic size. The AFM images shows that *n*-PACl reduced the surface roughness from 26.5 to 22.5 nm, which improved the uniformity of perovskite films (Fig. 8(a)).
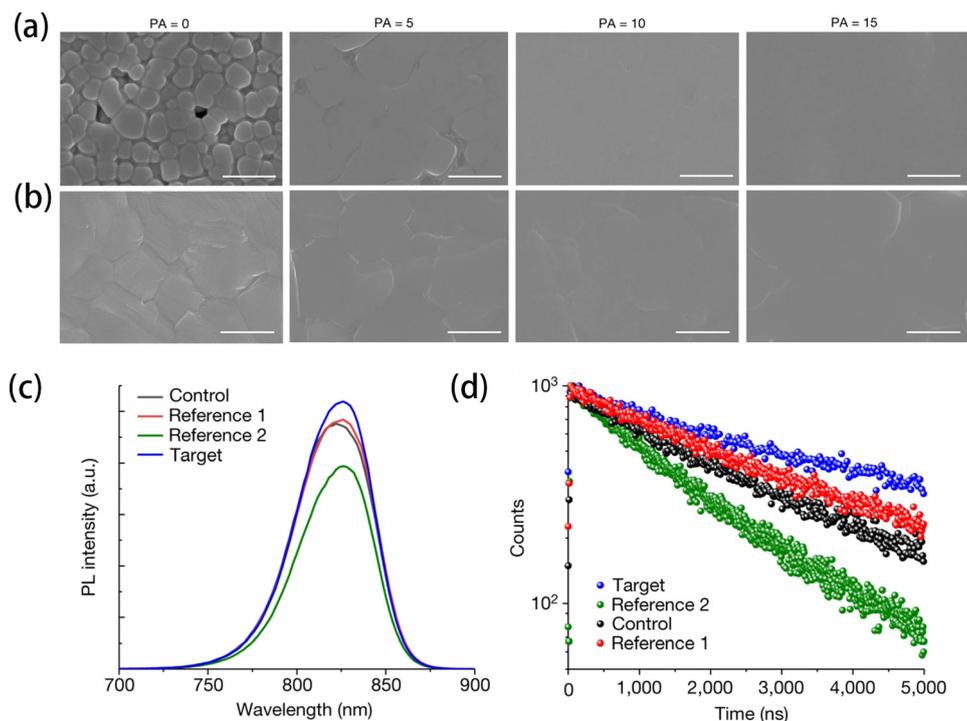
Fig. 7 SEM images of the surface morphologies of the perovskite thin films spin-coated with 0–15 mol% PACl added to the FAPbI$_3$ precursor containing 35 mol% MACl (a) without annealing and (b) with annealing. The scale bar is 1.0 μm. (c) Photoluminescence (PL) and (d) time-resolved photoluminescence (TRPL) spectra of the perovskite films deposited on a glass substrate. Reproduced from ref. 32 with permission from Springer Nature, copyright 2023.
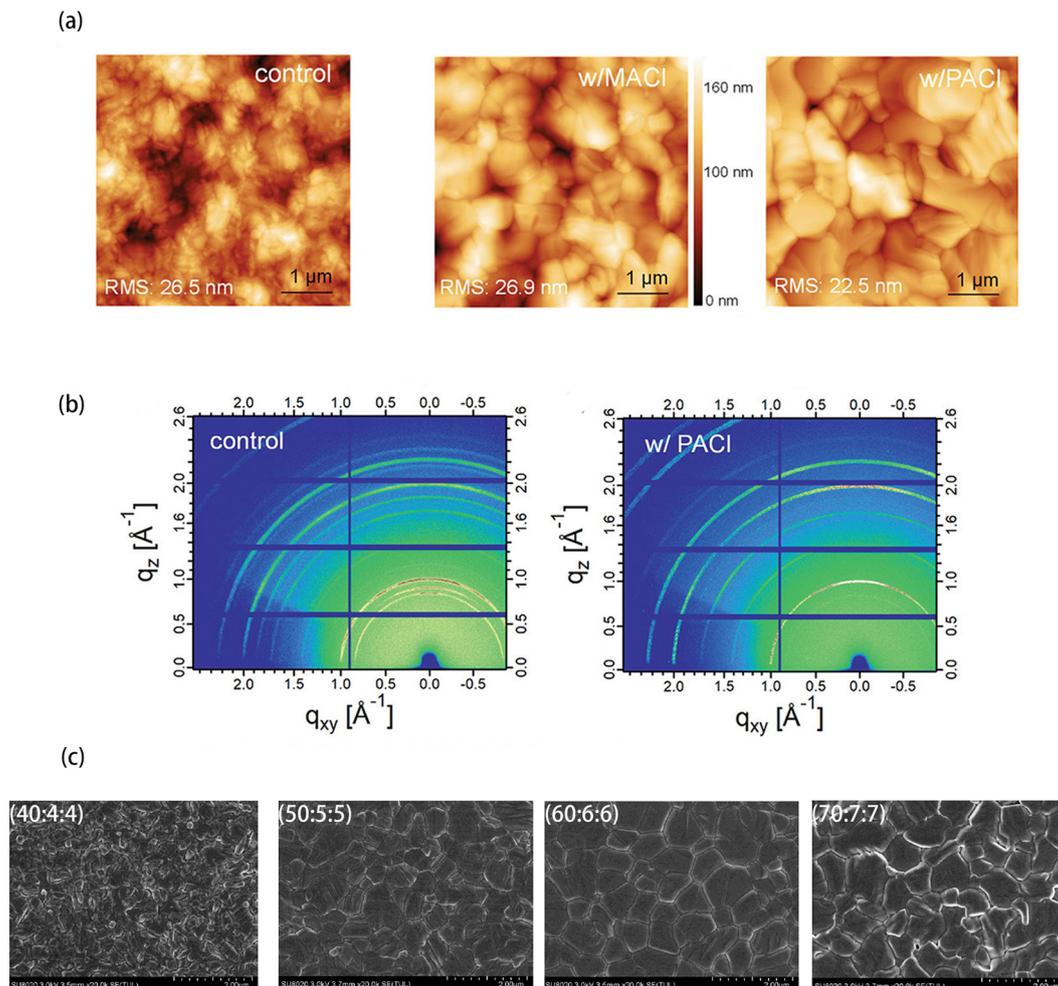
Fig. 8 (a) Atomic force microscopy (AFM) images of the perovskite films formed from the precursor solution without additive (control) and with additives of 20 mol% MACl or 20 mol% *n*-PACl. The scan size of the AFM images was 5 μm × 5 μm. (b) 2D Grazing-Incidence Wide-Angle X-ray Scattering (GIWAXS) patterns of the perovskite films without and with 20 mol% PACl. Reproduced from ref. 92 with permission from Wiley-VCH, copyright 2021. (c) SEM images of the perovskite films prepared with different precursor recipes. The scale bar is 2.0 μm. Reproduced from ref. 97 with permission from Multidisciplinary Digital Publishing Institute, copyright 2020.

Besides, the grain sizes of films with *n*-PACl were larger than that of the control films. Furthermore, the GIWAXS patterns are shown in Fig. 8(b). They compared the out-of-plane profile integrated scattering intensity in the q_z direction. The PbI$_2$ at $q_z = 0.9$ Å^{-1} disappeared and the δ-phase peak intensity at $q_z = 0.84$ Å^{-1} was reduced after adding the *n*-PACl additive. The intensity of the (100) plane of α-FAPbI$_3$ with *n*-PACl was twice that of the pristine film. Moreover, the patterns showed that the meridian out-of-plane (100) peak had the most intense scattering signal, which indicated the preferential crystal orientations for the α-phase FAPbI$_3$ in the perovskite film with *n*-PACl additive. The above analysis indicated that the perovskite film with *n*-PACl had better crystallinity and preferential crystal orientation than films without *n*-PACl. Benefiting from the improved film quality, the perovskite films with *n*-PACl had longer carrier lifetime and stronger PL intensity than that of the control films. Finally, the PCE of PVSCs with *n*-PACl could reach 22.22%, which was higher than the PCE of the control PVSCs (17.67%).

Tan *et al.* used an inorganic additive, ammonium halides (NH$_4$I), to improve the quality of cesium lead iodide (CsPbI$_3$) films.[93] In the pristine precursor solution, the Pb–I colloids could form and lead to uncontrollable nucleation. When NH$_4$I was introduced into precursor solution, the NH$_4$I could interact with Pb–I colloids to reduce their radius and then decrease the nucleation rate to adjust the growth process of the perovskite. In this way, the surface of CsPbI$_3$ films became more uniform, and the grain sizes became larger. Furthermore, the defect was suppressed and led to the reduction of nonradiative recombination. In this way, the carrier life time of CsPbI$_3$ films was improved from 2.1 ns (control film) to 15.7 ns (PVSCs with NH$_4$I). For the PVSCs performance, the PCE value was improved from 17.04% (control PVSCs) to 18.71% (PVSCs with NH$_4$I). Furthermore, the PVSCs with NH$_4$I can remain 96% of its initial PCE after 2000 h operation, which indicated its ultrahigh photoelectrical stability under continuous light illumination and relatively high bias voltage. The control PVSCs can only

retain 85% of its initial efficiency after 300 h under the same conditions.

To improve the film morphology and stability of Sn-based perovskite films under ambient conditions, S. Sandhu *et al.* used binary additives composed of 2-phenylethyl ammonium iodide (PEAI) and ethylene diammonium diiodide (EDAI$_2$) on formamidinium tin iodide (FASnI$_3$).[94] The EDAI$_2$ could reside on the grain boundaries as a bridge between adjacent perovskite crystals, while the PEAI worked as a spacer molecule between SnI$_6$ octahedra layers, forming the mixed 2D/3D perovskites. Therefore, the perovskite film with binary additives became more compact and stable with enlarged grains. With the addition of binary additives, the dark current was reduced by more than one order of magnitude, and the trap density was reduced from 1.78×10^{16} cm^{-3} to 0.95×10^{16} cm^{-3}. The PVSCs with the addition of binary additives achieved the champion PCE of 8.47%, which was significantly larger than the PCE of the control PVSCs (PCE = 3.64%).

Pseudo-halides have been also used as additives. Jeong *et al.* developed an anion engineering method, which used pseudo-halide anion, formate (HCOO$^-$), as the additive.[95] The HCOO$^-$ could strongly coordinate with undercoordinated Pb^{2+} cations, which helped to passivated the anion (I$^-$) vacancy, which are present at the grain boundaries and at the surface of the perovskite films. This strong coordination could also slow the growth process of perovskite, which led to enlarged stacked grains. The PVSCs fabricated by this method achieved a champion PCE of 25.6% (certified 25.2%) and 450 h stable operation time.

Tang *et al.* used a kind of 2D nonlayered materials called In$_2$S$_3$ nanoflakes (Nano-In$_2$S$_3$) as the additive.[96] With the addition of Nano-In$_2$S$_3$, not only the defects were passivated but the grain sizes of the perovskite films were also enlarged. The Nano-In$_2$S$_3$ had a random nanoflake that exhibits clear lattice fringes with a spacing of ≈ 3.2 Å, which could be assigned to the (311) planes of cubic β-In$_2$S$_3$ with an interplanar distance of 3.24 Å. These two values were very close to $d_{100} = 6.15$ Å of (100) plane and $d_{200} = 3.08$ Å of (200) plane in cubic α-CsPbI$_2$Br. Therefore, the lattice match was good. In addition, the In–S dangling bonds of nonlayered NanoIn$_2$S$_3$ could interact with the Pb^{2+} to form a Pb–S bond. Thus, the In$_2$S$_3$ additive could passivate the unsaturated Pb^{2+} defects. Therefore, according to the above analysis, the epitaxial growth of the perovskite film would be allowed, which could lead to larger grain sizes and improved crystallinity of the perovskite film. Furthermore, the film with the addition of NanoIn$_2$S$_3$ showed more uniform surface and larger grain sizes than that of the control films. Finally, the optimized PVSCs with NanoIn$_2$S$_3$ exhibited an enhanced PCE of 15.17%, which is considerably higher than that of the control PVSCs (13.17%).

In a similar scenario, Li *et al.* investigated the impact of MACl additive on the properties of perovskite films.[97] They set up several experiment groups with different concentrations of MACl of 40 : 4 : 4, 50 : 5 : 5, 60 : 6 : 6, and 70 : 7 : 7, which refer to the mass ratios of FAI, MABr, and MACl, which were 40 mg : 4 mg : 4 mg, 50 mg : 5 mg : 5 mg, 60 mg : 6 mg : 6 mg, and 70 mg : 7 mg : 7 mg, respectively. Fig. 8(c) shows that the grain sizes of the perovskite film first increased and then decreased as the concentration changed from 40 : 4 : 4 to 70 : 7 : 7. The 60 : 6 : 6 film exhibited the largest grain size among all the conditions. Besides, the 60 : 6 : 6 film was flat and free of pinholes. In contrast, the 40 : 4 : 4 film showed irregular morphology and its grains were small. For the 70 : 7 : 7 film, obvious pinholes can be seen, which confirms that the concentration of the precursors has a great impact on the morphology of FA$_x$MA$_{1-x}$Br$_x$Cl$_y$I$_{1-x-y}$ perovskite films.

Moreover, Li *et al.* developed another inorganic additive, carbon nitride (C$_3$N$_3$).[98] The C$_3$N$_3$ is an ultrathin 2D sheet-like material with a smooth surface. The C$_3$N$_3$ complexation energy with uncoordinated MA$^+$ and Pb^{2+} cations were -1.295 eV and -1.718 eV, and the bond length between C$_3$N$_3$ and MA$^+$ and Pb^{2+} cations were 1.887 Å and 2.875 Å, respectively. These indicated that the complexes of C$_3$N$_3$–MA$^+$ and C$_3$N$_3$–Pb^{2+} are easy to form. Therefore, when the C$_3$N$_3$ was added into the precursor solution, the C$_3$N$_3$ could interact with the uncoordinated Pb^{2+} and MA$^+$ and passivate the MA$^+$ and Pb^{2+} defects. With the addition of C$_3$N$_3$, the grain sizes of the perovskites became larger, and the charge recombination was suppressed. They also investigated the influence of concentration of C$_3$N$_3$ on PVSCs performance. The PCE of PVSCs first increased with the increase in the concentration of C$_3$N$_3$, then decreased. The PVSCs with 0.075 mg mL^{-1} showed the highest PCE of 19.91%, and the PCE of control PVSCs was only 18.16%.

In this section, we introduced typical methods of adding additives to the solution to regulate the crystallization reaction and ultimately improve the quality of perovskite films. These additives could interact with the solutes in the precursor solution, such as Pb^{2+} and I$^-$ in the FAPbI$_3$ precursor solution. Through these chemical reactions, we can control the nucleation and growth of perovskites, passivate the defects, and thus improve the performance of solar cells.

4. Mass transfer-controlled growth

Mass transfer refers to the process of transporting a substance from one place to another. During the crystallization process, molecules or ions migrate across precursors to aggregate and then constitute a perovskite crystal. Thus, the growth of perovskites could be adjusted by regulating the mass transfer process. For example, we could control the species of ions in the exchange reaction to change their migration speed, which should influence the formation rate of perovskites. Similarly, we could also change the pressure of molecules vapor to modulate the formation rate of perovskites. In this section, a certain number of methods for controlling the perovskite growth using mass transfer will be introduced. The main content will be divided into two parts: ion transfer and molecule transfer.

4.1 Ion transfer

Halide perovskites are ionic crystals, whose ions are relatively easy to move.[99] This feature could be used to fabricate the

perovskite films, such as ion exchange.[100–107] In this section, A-site cation exchange and X-site halogen anion exchange will be discussed.

    4.1.1 Cation exchange. For organic–inorganic perovskites, A-site ions are organic cations. Li *et al.* developed a FA^+/MA^+ cation exchange method to obtain high-quality Sn-based perovskite films, which improved the stability and efficiency of Sn-based PVSCs.[108] The route of $FASnI_3$ perovskite films growth is shown in Fig. 9(a). Firstly, formamidine acetate (FAAc) salt and

MAI were added into the precursor solution as dual cation sources instead of FAI. The FAAc and MAI could lead to the formation of mixed-cation $MA_xFA_{1-x}SnI_3$ perovskite films. During the annealing process, the MA cation in mixed perovskite could be replaced by free FA^+ cation from FAAc and form methylammonium acetate (MAAc), which then evaporated. Moreover, a higher annealing temperature could influence the ion exchange process and the evaporation of MAAc, and thus affect the film morphology and photoelectric property. Fig. 9(b) showed the SEM images of
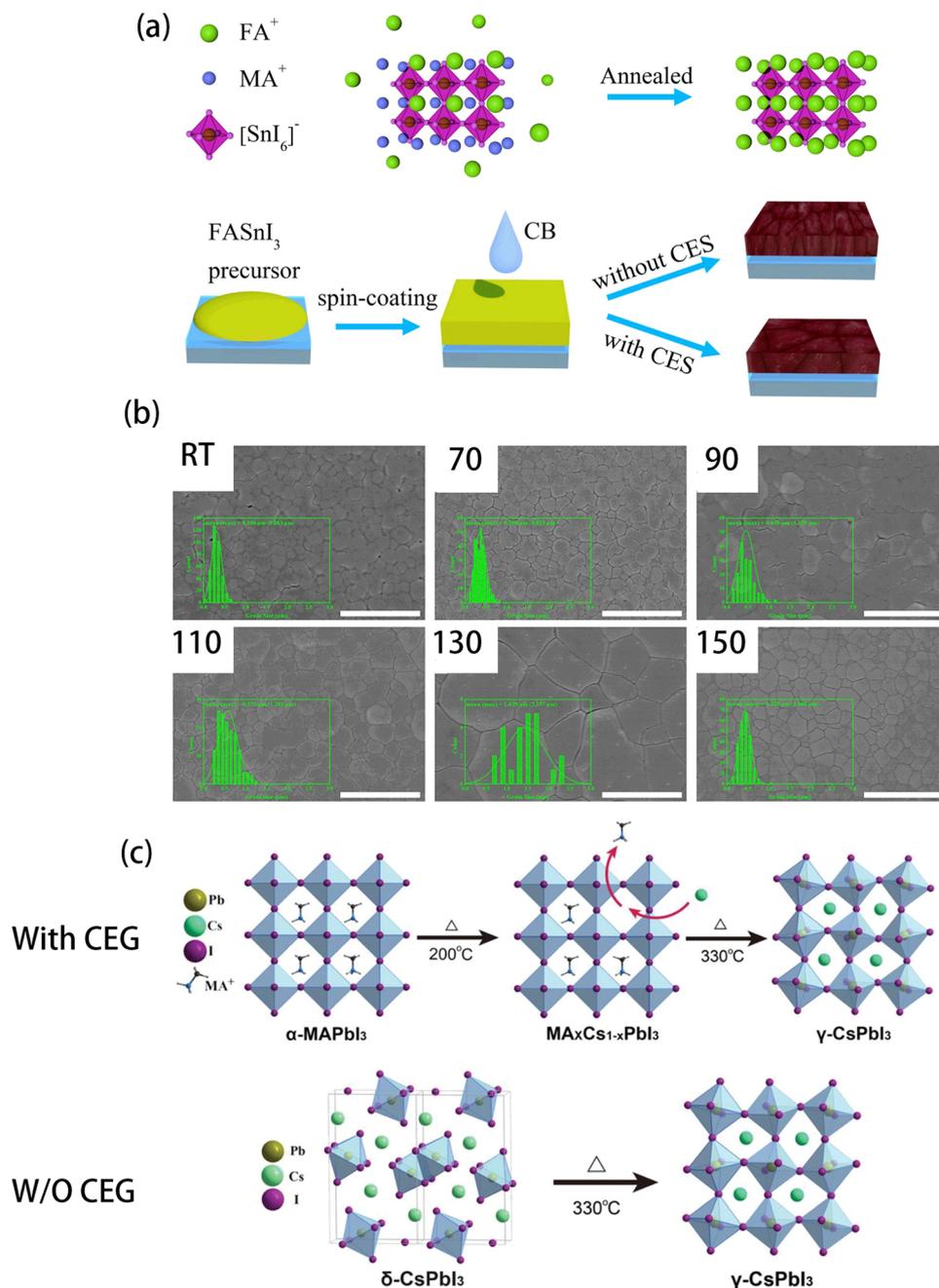
Fig. 9 (a) Schematic diagram of the cation exchange strategy (CES) method. (b) Top-view SEM images of FAAc-RT, FAAc-70 °C, FAAc-90 °C, FAAc-110 °C, FAAc-130 °C, and FAAc-150 °C perovskite films. The scale bar is 2 μm. Reproduced from ref. 108 with permission from American Chemical Society, copyright 2021. (c) Illustration of the $CsPbI_3$ crystal formation using the cation exchange growth (CEG) method and control method. Reproduced from ref. 112 with permission from Wiley-VCH, copyright 2019.

perovskite films with different annealing temperature. It is obvious that the grain sizes increased as the temperature increased from room temperature to 130 °C. Perovskite films with 130 °C annealing showed the largest grain sizes of 1.429 μm and a compact, uniform surface without pinholes. But, a very high temperature such as 150 °C could accelerate the evaporation rates, which could promote the nucleation of perovskite, resulting in smaller grain size. For photoelectric properties, the 130 °C perovskite film had the longest carrier lifetime (2.54 ns) and lowest lower trap density (2.90×10^{-15} cm^{-3}) among all the conditions. Accordingly, the Sn-based PVSC achieved an average PCE of $8.64 \pm 0.21\%$ and a champion PCE 9.11%. After 1320 h storage in dark in a glove box, the PVSCs could retain 80% of the initial PCE, which indicated the excellent stability.

Jeong *et al.* demonstrated a lamination-assisted bifacial cation exchange method to obtain high-quality perovskite film for flexible semitransparent PVSCs (ST-PSCs).[109] Two separate perovskite films (MAPbI$_3$ and FAPbI$_3$) were laminated in this method. During the lamination process, the FA and MA cations could exchange between two perovskite films. After the cation exchange, high-quality perovskite films with larger grain sizes and higher crystallinity than the control perovskite films were obtained. Accordingly, PVSCs with FA/MA cation exchange reach a champion PCE of 15.1%.

For mixed-cation PVSCs, Shao *et al.* developed a Cs$_4$PbI$_6$-mediated method to synthesize Cs-rich FA$_x$Cs$_{1-x}$PbI$_3$.[110] They first introduced excess FAI in the precursor solution and annealed the film at 100 °C. Both Cs$_4$PbI$_6$ and FA-rich FA$_x$Cs$_{1-x}$PbI$_3$ were formed during the 100 °C annealing process. In the next annealing process at 220 °C, the fast FA$^+$/Cs$^+$ exchange took place between Cs$_4$PbI$_6$ and FA-rich FA$_x$Cs$_{1-x}$PbI$_3$ perovskite to form Cs-rich FA$_x$Cs$_{1-x}$PbI$_3$ because of the lower ion diffusion barrier of Cs$_4$PbI$_6$. For the PVSCs performance, PVSCs fabricated by this method showed a V_{oc} of 1.02 V, J_{sc} of 21.4 mA cm^{-2}, FF of 80.0%, and a champion PCE of 17.5%. After storing in a dry box at room temperature and RH of 20% for 300 h, the PVSCs fabricated by this method could retain 87% of the initial PCE, which indicated the higher stability than the control CsPbI$_3$ PVSCs.

Ion exchange can induce phase conversion. Miao *et al.* synthesized a 1D perovskite, (pyrrolidinium)PbI$_3$, with orthorhombic phase.[111] Then, the 1D perovskite was put in CH$_3$NH$_2$ (MA) atmosphere to transform to the 3D MAPbI$_3$ perovskite. The cation exchange reaction is as follows.

$$C_4NH_{10}PbI_3(s) + CH_3NH_2(g) \rightarrow CH_3NH_2PbI_3(s) + C_4NH_9(g) \tag{1}$$
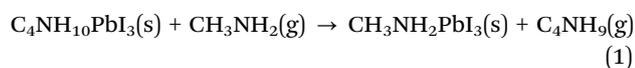
The transformed MAPbI$_3$ films showed a dense and compact surface with larger grain sizes up to ≈ 1 μm than that of 1D (pyrrolidinium) PbI$_3$. For the PVSCs performance, a champion PCE of 19.2% was achieved.

In inorganic perovskite, A-site ions are metal cations. Lau *et al.* developed a cation exchange growth (CEG) method to obtain high-quality CsPbI$_3$ by adding MAI in the precursor solution.[112] Fig. 9(c) shows the procedure of this CEG method. The MAPbI$_3$ perovskite was formed firstly because of the

addition of MAI, which acted as a perovskite template for subsequent ion exchange. In the subsequent annealing process, the MA$^+$ ions in the MAPbI$_3$ could be replaced by Cs$^+$ in the precursor solution to form the γ-phase CsPbI$_3$ perovskite. Using this method, a champion PCE of 14.1% was obtained, which was significantly higher than the PCE of the control PVSCs (PCE = 9.8%).

4.1.2 Anion exchange. X-site ions in perovskite could be I$^-$, Br$^-$, and Cl$^-$, which move much faster than the cations. Thus, the X-site ion exchange showed significant difference to A-site ion exchange.

To obtain high quality Cs$_{0.14}$FA$_{0.86}$Pb(Br$_x$I$_{1-x}$)$_3$ with proper I$^-$/Br$^-$ ratio, Niu *et al.*[113] developed a vapor–solid reaction employing alkali–metal ions (Na$^+$, K$^+$, Rb$^+$) to regulate the halogen ion-exchange process. The schematic illustration is shown in Fig. 10(a). They first deposited cesium bromide (CsBr)/PbI$_2$ inorganic frameworks with different alkali metal iodide (NaI, KI, and RbI). Then, the frameworks were treated in FAI/FACl mixed vapor. The Cl$^-$ with high migration speed transformed the frameworks into perovskite films *via* Cl$^-$/Br$^-$ ion exchange. Then, the Cl will release in the form of FACl at high temperature. In this process, the alkali metal cations reacted with the halogen anion through Coulomb force to inhibit the movement of halogen anion, thus allowing the perovskite films to reach a proper amount of Br. Proper ion exchange could improve the film morphology and photoelectric property. Fig. 10(b) showed the SEM images of perovskite films with alkali metal iodides. When NaI, KI, and RbI were added, perovskite films showed large grain sizes (from 600 nm to 1 μm), while the control films only showed small grain sizes of about 400 nm. Finally, the PCE of the PVSCs was increased from 17.3% for the control PVSCs to 19.6% for the PVSCs using this method. In the same way, Ding *et al.* developed a vapor–solid reaction, which used MAI or FAI vapor to react with crystalline film and led to the ion exchange between Cl$^-$ and I$^-$.[114]

Solid–solid and solid–liquid reaction are also good ways to achieve ion exchange between halogen ions. Zhang *et al.* reported a slow ion exchange method by physically pairing CsPbIBr$_2$ and MAPbI$_3$ films.[115] The schematic illustration of this slow ion exchange is shown in Fig. 10(c). When the temperature increased, the Br$^-$ and I$^-$ could slowly exchange, which form CsPbI$_{1+x}$Br$_{2-x}$ and MAPbI$_{3-x}$Br$_x$ films. Furthermore, the grain sizes of CsPbI$_{1+x}$Br$_{2-x}$ films became larger with increasing ion exchange time. The root-mean-square (RMS) of CsPbI$_{1+x}$Br$_{2-x}$ were 22.3, 19.4, 18.7, and 15.5 nm with ion exchange time of 0, 1, 2, and 3 h, respectively. This meant that the surface of the perovskite film became smoother with increasing ion exchange time. The best-performing PVSCs that used this method showed a PEC of 10.94%, which was higher than the PCE of PVSCs fabricated with the pristine CsPbIBr$_2$ film (8.21%).

Wu *et al.* developed a halogen ion-exchange method to obtain mixed-halide double perovskite Cs$_2$AgBiBr$_{6-x}$I$_x$ by dropping MAI solution onto Cs$_2$AgBiBr$_6$ perovskite films.[116] The solid–liquid reaction could take place between MAI solution
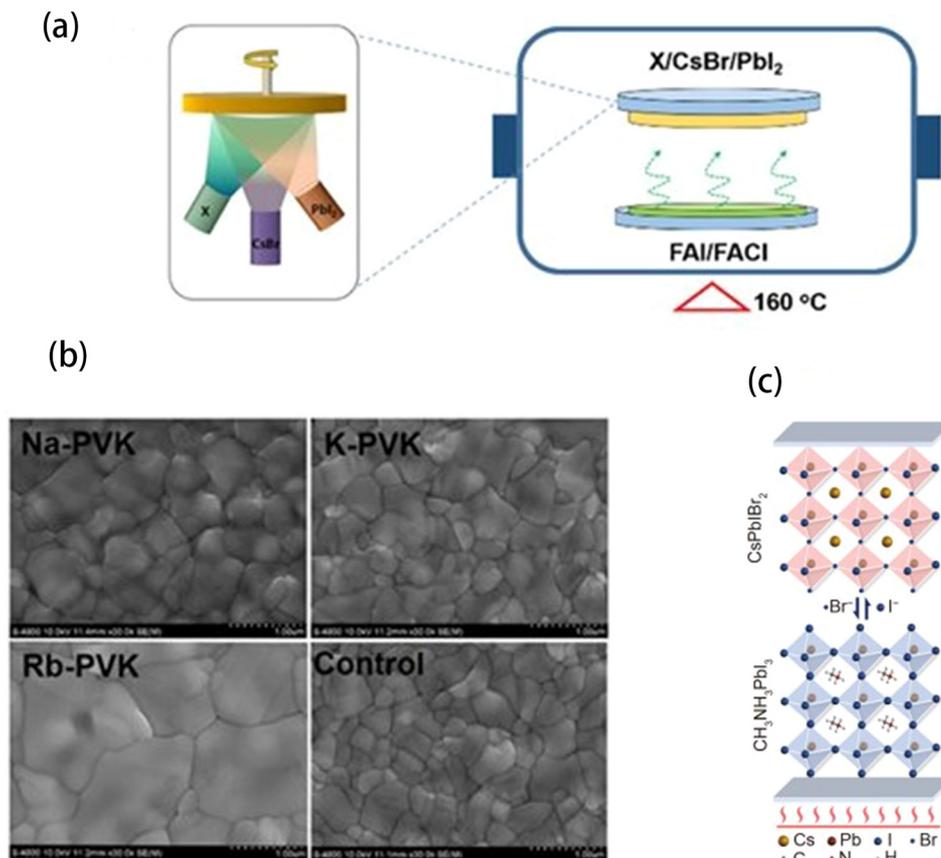
Fig. 10 (a) Schematic illustration of the vapor–solid reaction process. (b) SEM images of the control, Na-PVK, K-PVK, and Rb-PVK films. Reproduced from ref. 113 with permission from Wiley-VCH, copyright 2021. (c) Schematic illustration of the halide exchange strategy with a slow reaction rate. Reproduced from ref. 115 with permission from Springer Nature, copyright 2021.

and $Cs_2AgBiBr_6$ perovskite film, which could induce ion exchange between Br^- and I^- and lead to the formation of $Cs_2AgBiBr_{6-x}I_x$. In another work, Jiao *et al.* synthesized a 1D single crystal $FA_4Pb_3I_6Ac_4$ and then react with MAI solution.[117] In this way, the I^- from MAI could exchange with CH_3COO^- (Ac^-) from $FA_4Pb_3I_6Ac_4$ to form 3D black α-phase $FAPbI_3$. The modified perovskite film showed a compact surface and small grain sizes with few pinholes. The modified film also showed longer carrier (784 ns) lifetime than that of the control film (499 ns), which indicated the low trap density of the modified perovskite films. The PVSCs with modified perovskite films achieved a champion PCE of 23.65%, while the PCE of the control PVSCs was 22.48%.

To obtain high-performance $CsPbI_2Br$ PVSCs, Shan *et al.* developed a combined method of nonstoichiometric composition and post-cation exchange.[118] In their work, nonstoichiometric composition means that they adjusted the composition of precursor solution with excess PbI_2 (marked as NS-films, short for nonstoichiometric). The excess PbI_2 could adjust the precipitation and crystal growth process during spin coating. For the performance of PVSCs, as the PbI_2 composition increased, the FF first increased then decreased, indicating that the series resistance (R_s) first decreased then increased. The PVSCs with 5% excess PbI_2 showed the best PCE of 16.36% while the control PVSCs showed PCE of 14.73%. However, the PVSCs with excess PbI_2 still had the instability problem such as bad stabilized power output (SPO). To solve this issue, they capped the perovskite surface with FAI to passivate the defect and improve the quality of perovskite films. The FAI could react with perovskite on the top surface and grain boundary to form I^--rich and FA^+-containing lattice. When extending the annealing time, FA^+ proceed into the bulk crystal *via* ion exchange between FA^+ and Cs^+, which improved charge extraction and suppressed the carrier's recombination of PVSCs. Benefiting from the combined methods of nonstoichiometric composition and post-cation exchange, the PVSCs achieved the champion PCE of 17.80%, which is the record PCE of $CsPbI_2Br$-based PVSCs so far.

In this section, we discussed ion-exchange methods to fabricate perovskite films, including cation exchange and anion exchange. The difference between these two methods lies in the movement speed of ions. For inorganic and organic mixed perovskite, the ion at A-site is an organic cation, and its movement speed is slower than that of the anion at X-site, which makes the above two methods different in practical applications. Thus, the X-site anion exchange can take place quickly at room temperature and easy to apply to the fabrication of PVSCs. At the same time, not only single component perovskite

film but also mixed perovskite film can be manufactured by the ion-exchange method. The ion-exchange method can also be used in many cases because the exchange reactions can occur in liquid–liquid, gas–solid, solid–liquid, and solid–solid.

4.2 Molecule transfer

Molecules and ions are different in some of their properties, such as their sizes and charges. As a result, molecular transfer is very different from ion transfer. Since molecules are electrically neutral and ions are charged, ions can be moved by electric fields, whereas molecules can only be moved by concentration gradients or by certain devices or carriers. By molecular transfer, such as the vapor deposition, we can accurately control the thickness and quality of perovskite films and produce high-quality perovskite film. Vapor deposition includes vacuum deposition and chemical vapor deposition. Vacuum deposition usually requires a high vacuum, but chemical vapor deposition usually operates under low pressure or even close to ambient pressure.

Perovskite films produced by vacuum deposition had uniform and large grain sizes, which was first realized in 2013.[119] In the following research, Arivazhagan et al. applied a similar vacuum co-deposition method to produce high-quality $MAPbI_3$ films.[120] The scheme of vacuum co-deposition method is shown in Fig. 11(a). The two source materials of MAI and PbI_2 were placed in two crucibles and heated to produce vapor. The vapor of MAI and PbI_2 could contact the glass substrate together and form $MAPbI_3$ films. The pressure had great impact on the perovskite film and is easy to control. Fig. 11(b)–(e) shows SEM images of $MAPbI_3$ with different deposition pressures and temperatures of the MAI source, which were $7.5 \pm 0.3 \times 10^{-4}$ Pa (125 °C), $1.5 \pm 0.3 \times 10^{-3}$ Pa (150 °C), $4.5 \pm 0.3 \times 10^{-3}$ Pa (175 °C), and $7.5 \pm 0.3 \times 10^{-3}$ Pa (175 °C), respectively. The grain sizes of the perovskite films increased and the films became denser as the pressure increased from

$7.5 \pm 0.3 \times 10^{-4}$ Pa to $4.5 \pm 0.3 \times 10^{-3}$ Pa. However, the perovskite film with $7.5 \pm 0.3 \times 10^{-3}$ Pa pressure showed a mass of small grains, which is located at the grain boundaries. This indicated that a very high pressure could damage the film morphology. Accordingly, the perovskite films with $4.5 \pm 0.3 \times 10^{-3}$ Pa pressure showed the highest carrier life time of 31 ns among all the samples. They also showed better crystallinity than that of the perovskite films with $7.5 \pm 0.3 \times 10^{-4}$ Pa and $1.5 \pm 0.3 \times 10^{-3}$ Pa pressures but were same as the films with $7.5 \pm 0.3 \times 10^{-3}$ Pa pressure. The PVSCs fabricated at a pressure of $4.5 \pm 0.3 \times 10^{-3}$ Pa showed the best PCE of 15.74%.

Through the similar route, many kinds of perovskite films were produced for PVSCs by vacuum deposition. Escrig et al. designed a four-source vacuum deposition process to obtain $FA_{1-n}Cs_nPb(I_{1-x}Br_x)$ perovskite film with wide bandgap and controlled morphology, which used FAI, CsI, PbI_2, and $PbBr_2$ as the sources.[121] To obtain the $MAPb_{3-x}Cl_x$ perovskite film, Babaer et al. used three-source vacuum deposition, which included MAI, PbI_2, and $PbCl_2$.[122] They found out that $MAPb_{3-x}Cl_x$ showed high electroluminescence efficiency, long PL lifetimes, and large photovoltage because of the existence of chloride. The incorporation of chloride could reduce the trap density and thus suppressed the nonradiative recombination. For the PVSCs performance, the PVSCs fabricated by this method achieved a champion PCE of 16.1%.

However, the high vacuum that vacuum deposition usually needs has already become a disadvantage because of its high cost. But chemical vapor deposition (CVD) only requires low pressure or even ambient condition, which should be relatively cost-effective. In 2016, Yin et al. used the CVD method to produce $MAPbI_3$ films.[123] The schematic illustration of their experimental setup is shown in Fig. 12(a). The MAI vapor was transported alone in the chamber driven by the carrier gas. In this way, the MAI vapor could move into PbI_2 film to form $MAPbI_3$ film. With this method, the perovskite films showed a
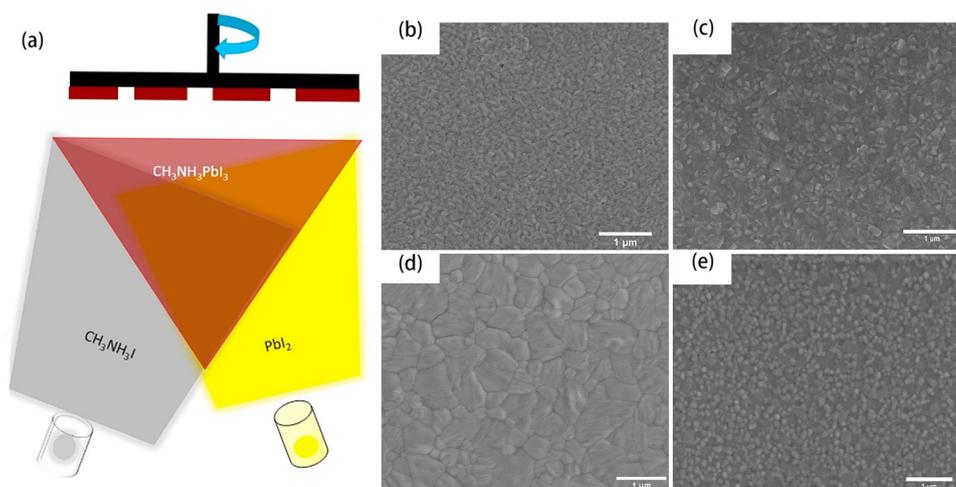
Fig. 11 (a) Schematic illustration of the pressure-controlled co-deposition method. (b)–(e) SEM images of $MAPbI_3$ thin films prepared at different pressures. (b) $7.5 \pm 0.3 \times 10^{-4}$ Pa (125 °C), (c) $1.5 \pm 0.3 \times 10^{-3}$ Pa (150 °C), (d) $4.5 \pm 0.3 \times 10^{-3}$ Pa (175 °C), and (e) $7.5 \pm 0.3 \times 10^{-3}$ Pa (175 °C). The scale bar is 1 μm. Reproduced from ref. 120 with permission from Elsevier, copyright 2019.
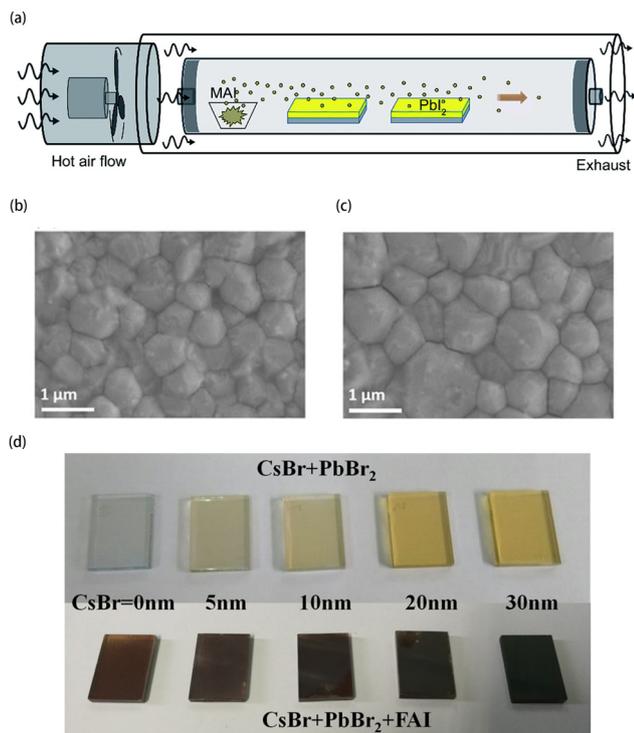
Fig. 12 (a) Schematic illustration of the ambient atmosphere vapor-assisted deposition equipment. Reproduced from ref. 123 with permission from Royal Society of Chemistry, copyright 2016. Top-view SEM images of Pb (b) and Pb–In-based (c) perovskite films. Reproduced from ref. 124 with permission from Wiley-VCH, copyright 2022. (d) Photograph of the CsBr/PbBr$_2$ film and the mixed-cation perovskite films. Reproduced from ref. 125 with permission from Elsevier, copyright 2018.

dense and uniform surface. For the PVSCs performance, a high PCE of 18.90% of PVSCs was achieved.

In another work, Tavakoli *et al.* developed a CVD method to grow lead–indium (Pb–In)-based perovskite films, which used metal alloying of halide-perovskite domain *via* ion-transfer (MAHDI).[124] This method allows them to replace toxic Pb metal with other metals. They first produced Pb–In alloy thin films, then placed the metal films in the middle of a tube. The MAI source was heated to 180 °C to produce MAI vapor. This MAI vapor was driven by argon gas to contact metal films to grow perovskites. Fig. 12(b) and (c) shows the SEM images of Pb-based and Pb–In-based perovskite films. These images indicated that the Pb–In-based perovskite films had large average grain sizes of 920 nm but the Pb-based perovskite films' average grain sizes was only 780 nm. This method also improved the crystallinity and PL of perovskite films. Finally, the PVSCs made by this method achieved a maximum PCE of 21.2%.

Using a similar route, mixed-perovskite films could be produced by CVD. Tong *et al.* developed a precisely tunable stack sequence physical–chemical vapor deposition (SS-PCVD) method.[125] In this way, they successfully produced $Cs_{0.15}FA_{0.85}PbI_{2.85}Br_{0.15}$ perovskite films with a gradient distribution of Cs ions. They firstly deposited CsBr and PbBr$_2$ on substrates. Then, CsBr + PbBr$_2$ films were put into a CVD system to react

with FAI vapor and subsequently to form perovskite films. At room temperature, α-phase FA-perovskite could transfer into the β-phase, which is bad for the stability of PVSCs. With the existent of Cs cations, the mixed perovskite films could be stabilized at black α-phase (Fig. 12(d)). Using this method, the PVSCs based on the $Cs_{0.15}FA_{0.85}PbI_{2.85}Br_{0.15}$ film showed a relatively higher PCE of 18.22% than that of FAPbI$_3$ (PCE = 11.69%) and MAPbI$_3$ (PCE = 15.10%).

In this section, two typical methods of vapor deposition are introduced: (1) vacuum deposition and (2) chemical vapor deposition. The differences between the two methods are as follows: vacuum deposition requires a higher vacuum and has higher requirements of equipment; chemical vapor deposition, on the other hand, does not require a high vacuum and can be carried out even in ambient environments. Due to the simple requirements for the production of perovskite films by chemical vapor deposition, it has become one of the most desirable manufacturing methods for perovskite films. The advantage of vacuum deposition is that the thickness of the perovskite film can be precisely controlled.

5. Summary and outlook

In this review article, we have discussed and summarized three kinds of strategies to synthesize high quality perovskite films, including the crystallization reaction-controlled growth, additive-controlled growth, and mass transfer-controlled growth.

The crystallization reaction-controlled growth includes the "intermediate engineering" part and the "reaction conditions" part. Engineering the intermediates is a powerful route to control the crystallization of films by regulating the formation process of intermediates. In this way, we can delay the crystallization rate of halide perovskites. As a result, it can increase the grain size of films, make the surface compact, and improve the crystallinity. In the reaction condition part, we introduce three reaction conditions, including temperature, pressure, and concentration of perovskite precursor solutions. Their effects on the film's crystallization reaction are discussed. Then we introduce several typical methods to improve the quality of perovskite films by controlling the three reaction conditions. Through this route, we can effectively control the crystallization rate of perovskite films, improve the solubility of the solute in the precursor solution, and make the surface of the perovskite film smooth and compact. Finally, the defects of the film are reduced, and the performance of the corresponding PVSCs is improved.

In the additive-controlled growth section, we introduce typical additives and their effects on perovskite films, including organic and inorganic additives. During the crystallization of perovskite films, these additives can react with the precursors or perovskite through their functional groups or atoms and thus passivate the uncoordinated bonds, increase the carrier lifetime, and improve the films' stability. Furthermore, with the help of additives, the crystallization rate of the films is

regulated and the surface morphology of the films is improved. Finally, high-performance PVSCs have been achieved, whose PCE exceeded 25.7% through additive engineering.

Unlike the above two strategies, mass transfer is more like a physical process. In this section, we introduce ion and molecular mass transfer-controlled growth of halide perovskites. Both ions and molecules can be moved by concentration differences. But ions are charged and molecules are not, which allows ions to move when driven by an electric field.

In the ion transfer part, we focus on ion exchange, which is a classical method to control crystal growth. Ion transfer can occur not only between liquid and liquid but also between solid and liquid, liquid and gas, *etc.* The A-site cation exchange and X-site anion exchange of perovskite are discussed, respectively. By ion transfer, it is possible to produce not only single component perovskites of high quality but also mixed perovskites of high quality. In this way, we can regulate the band gap of perovskites, increase the grain size and crystallinity of the films, and make the film smooth and compact. Moreover, the trap density is reduced and the carrier lifetime is enlarged.

In the molecule transfer part, we focus on vapor deposition. Vapor deposition is divided into vacuum deposition and chemical vapor deposition. Vacuum deposition can accurately control the thickness of perovskite films and improve their quality, with accurate control of the gas generation rate. But this technology is expensive and requires an extremely high vacuum, with relatively low growth rates. Chemical vapor deposition, however, does not require a very high vacuum and can be carried out at low pressure or even close to ambient temperature. Also, its manipulation is easy and suitable for deposition of large area of perovskite films. This technology has become one of the promising perovskite film manufacturing technologies.

At present, the main goals of research for PVSCs are improving their efficiency, enhancing stability, and reducing cost.[126,127] As for the fabrication strategies mentioned in this review, there are several development directions of PVSCs as follows.

(1) In the field of intermediate engineering, first of all, the mechanism of the influence of intermediate phases on perovskite thin films should be further studied. Various instruments, such as XRD, SEM, and GIWAXS, should be used to *in situ* characterize the conversion process of intermediates to perovskites. Secondly, advanced intermediate engineering strategies should be designed for the robust production of high-quality perovskite films in the ambient environment.

(2) The combination of additive engineering and other types of strategies is an important development direction. For example, additive engineering can be combined with intermediate engineering. Some additives can form complexes with perovskite precursors to regulate the growth of perovskite films. But, at the same time, there still remain problems to be solved for additive engineering, such as the reaction of the additive with the perovskite, the relationship between the additives and the stability improvement of the perovskite film, and the difficulty of commercialization due to the high cost of some additives.

(3) For chemical vapor deposition, techniques should be developed to enable large area perovskite films deposition at a low cost. To achieve this, the uniformity of film deposition should be carefully optimized. Besides, precursors should be customized for vapor phase crystallization reactions, which should further improve the quality of perovskite films for PV.

Author contributions

S. Xiao and C. Zhou supervise the project. S. Xiao and X. Xie develop the conceptualization. X. Xie and S. Zeng write the original draft. S. Xiao review and edit the manuscript.

Conflicts of interest

There are no conflicts of interest to declare.

Acknowledgements

References

1 Solar PV power generation in the Net Zero Scenario. https://www.iea.org/data-and-statistics/charts/solar-pv-power-generation-in-the-net-zero-scenario-2010-2030.

2 L. Duan, D. Walter, N. Chang, J. Bullock, D. Kang, S. P. Phang, K. Weber, T. White, D. Macdonald, K. Catchpole and H. Shen, Stability Challenges for the Commercialization of Perovskite–Silicon Tandem Solar Cells, *Nat. Rev. Mater.*, 2023, **8**, 261–281.

3 Best-research-cell-efficiencies. https://www.nrel.gov/pv/assets/pdfs/best-research-cell-efficiencies.pdf.

4 Z. Li, B. Li, X. Wu, S. A. Sheppard, S. Zhang, D. Gao, N. J. Long and Z. Zhu, Organometallic-Functionalized Interfaces for Highly Efficient Inverted Perovskite Solar Cells, *Science*, 2022, **376**, 416–420.

5 N. G. Park and K. Zhu, Scalable Fabrication and Coating Methods for Perovskite Solar Cells and Solar Modules, *Nat. Rev. Mater.*, 2020, **5**, 333–350.

6 N. J. Jeon, J. H. Noh, W. S. Yang, Y. C. Kim, S. Ryu, J. Seo and S. Il Seok, Compositional Engineering of Perovskite Materials for High-Performance Solar Cells, *Nature*, 2015, **517**, 476–480.

7 J. Burschka, N. Pellet, S. J. Moon, R. Humphry-Baker, P. Gao, M. K. Nazeeruddin and M. Grätzel, Sequential Deposition as a Route to High-Performance Perovskite-Sensitized Solar Cells, *Nature*, 2013, **499**, 316–319.

8   D. Bi, W. Tress, M. I. Dar, P. Gao, J. Luo, C. Renevier, K. Schenk, A. Abate, F. Giordano, J. P. Correa Baena, J. D. Decoppet, S. M. Zakeeruddin, M. K. Nazeeruddin, M. Grätzel and A. Hagfeldt, Efficient Luminescent Solar Cells Based on Tailored Mixed-Cation Perovskite, *Sci. Adv.*, 2016, **2**, e1501170.

9   S. Xiao, F. Xu, Y. Bai, J. Xiao, T. Zhang, C. Hu, X. Meng, H. Tan, H. P. Ho and S. Yang, An Ultra-Low Concentration of Gold Nanoparticles Embedded in the NiO Hole Transport Layer Boosts the Performance of p-i-n Perovskite Solar Cells, *Sol. RRL*, 2019, **3**, 1800278.

10 S. Xiao, H. Chen, F. Jiang, Y. Bai, Z. Zhu, T. Zhang, X. Zheng, G. Qian, C. Hu, Y. Zhou, Y. Qu and S. Yang, Hierarchical Dual-Scaffolds Enhance Charge Separation and Collection for High Efficiency Semitransparent Perovskite Solar Cells, *Adv. Mater. Interfaces*, 2016, **3**, 1600484.

11 R. Zhao, K. Zhang, J. Zhu, S. Xiao, W. Xiong, J. Wang, T. Liu, G. Xing, K. Wang, S. Yang and X. Wang, Surface Passivation of Organometal Halide Perovskites by Atomic Layer Deposition: An Investigation of the Mechanism of Efficient Inverted Planar Solar Cells, *Nanoscale Adv.*, 2021, **3**, 2305–2315.

12 J. Dou, Y. Bai and Q. Chen, Challenges of Lead Leakage in Perovskite Solar Cells, *Mater. Chem. Front.*, 2022, **6**, 2779–2789.

13 S. Xiao, W. Qian and S. Yang, Interfaced Structures between Halide Perovskites: From Basics to Construction to Optoelectronic Applications, *Adv. Energy Mater.*, 2022, 2201472.

14 H. Zhang and N.-G. Park, Polarons in Perovskite Solar Cells: Effects on Photovoltaic Performance and Stability, *J. Phys. Energy*, 2023, **5**, 024002.

15 X. Chu, Q. Ye, Z. Wang, C. Zhang, F. Ma, Z. Qu, Y. Zhao, Z. Yin, H.-X. Deng, X. Zhang and J. You, Surface *in Situ* Reconstruction of Inorganic Perovskite Films Enabling Long Carrier Lifetimes and Solar Cells with 21% Efficiency, *Nat. Energy*, 2023, **8**, 372–380.

16 Y. He, Z. Lin, J. Wang, K. Zhang, X. Xu, Y. Li, X. Huang, T. Ma, S. Xiao and S. Yang, A Heat-Liquefiable Solid Precursor for Ambient Growth of Perovskites with High Tunability, Performance and Stability, *Small Methods*, 2022, **6**, 2200384.

17 D. He, L. Shen, Y. Bai and L. Wang, Rational Strategies toward Efficient and Stable Lead-Free Tin Halide Perovskite Solar Cells, *Mater. Chem. Front.*, 2021, **5**, 4107–4127.

18 K. Zhang, Z. Wang, G. Wang, J. Wang, Y. Li, W. Qian, S. Zheng, S. Xiao and S. Yang, A Prenucleation Strategy for Ambient Fabrication of Perovskite Solar Cells with High Device Performance Uniformity, *Nat. Commun.*, 2020, **11**, 1006.

19 Y. Deng, H. Liu, H. Wang, Y. Song, W. Li, L. Zhu, X. Xie, S. Xiao and H. Chen, Carbon-Based Sb$_2$(S, Se)$_3$ Solar Cells., *Inorganics*, 2023, **11**, 159.

20 S. Xiao, K. Zhang, S. Zheng and S. Yang, Good or Evil: What Is the Role of Water in Crystallization of Organometal Halide Perovskites?, *Nanoscale Horiz.*, 2020, **5**, 1147–1154.

21 Z. Zhang, C. Wang, F. Li, L. Liang, L. Huang, L. Chen, Y. Ni, P. Gao and H. Wu, Bifunctional Cellulose Interlayer Enabled Efficient Perovskite Solar Cells with Simultaneously Enhanced Efficiency and Stability, *Adv. Sci.*, 2023, **10**, 2207202.

22 C. Jiang, J. Zhou, H. Li, L. Tan, M. Li, W. Tress, L. Ding, M. Grätzel and C. Yi, Double Layer Composite Electrode Strategy for Efficient Perovskite Solar Cells with Excellent Reverse-Bias Stability, *Nano-Micro Lett.*, 2023, **15**, 12.

23 H. Zhong, X. Liu, M. Liu, S. Yin, Z. Jia, G. Fu, S. Yang and W. Kong, Suppressing the Crystallographic Disorders Induced by Excess PbI$_2$ to Achieve Trade-off between Efficiency and Stability for PbI$_2$-Rich Perovskite Solar Cells, *Nano Energy*, 2023, **105**, 108014.

24 N. Li, X. Niu, L. Li, H. Wang, Z. Huang, Y. Zhang, Y. Chen, X. Zhang, C. Zhu, H. Zai, Y. Bai, S. Ma, H. Liu, X. Liu, Z. Guo, G. Liu, R. Fan, H. Chen, J. Wang, Y. Lun, X. Wang, J. Hong, H. Xie, D. S. Jakob, X. G. Xu, Q. Chen and H. Zhou, Liquid Medium Annealing for Fabricating Durable Perovskite Solar Cells with Improved Reproducibility, *Science*, 2021, **373**, 561–567.

25 M. Kim, G. H. Kim, T. K. Lee, I. W. Choi, H. W. Choi, Y. Jo, Y. J. Yoon, J. W. Kim, J. Lee, D. Huh, H. Lee, S. K. Kwak, J. Y. Kim and D. S. Kim, Methylammonium Chloride Induces Intermediate Phase Stabilization for Efficient Perovskite Solar Cells, *Joule*, 2019, **3**, 2179–2192.

26 S. Xiao, Y. Bai, X. Meng, T. Zhang, H. Chen, X. Zheng, C. Hu, Y. Qu and S. Yang, Unveiling a Key Intermediate in Solvent Vapor Postannealing to Enlarge Crystalline Domains of Organometal Halide Perovskite Films, *Adv. Funct. Mater.*, 2017, **27**, 1604944.

27 Y. Li, Z. Lin, J. Wang, R. Xu, K. Zhang, G. Wang, T. Liu, H. Zhou, S. Xiao and S. Yang, Amine Salts Vapor Healing Perfected Perovskite Layers for NiOx Based P-i-n Solar Cells, *Adv. Funct. Mater.*, 2022, **32**, 2203995.

28 S. Xiao, Y. Li, S. Zheng and S. Yang, Post-Treatment Techniques for High-Performance Perovskite Solar Cells, *MRS Bull.*, 2020, **45**, 431–438.

29 Z. Xiao, Q. Dong, C. Bi, Y. Shao, Y. Yuan and J. Huang, Solvent Annealing of Perovskite-Induced Crystal Growth for Photovoltaic-Device Efficiency Enhancement, *Adv. Mater.*, 2014, **26**, 6503–6509.

30 J. You, Y. (Michael) Yang, Z. Hong, T.-B. Song, L. Meng, Y. Liu, C. Jiang, H. Zhou, W.-H. Chang, G. Li and Y. Yang, Moisture Assisted Perovskite Film Growth for High Performance Solar Cells, *Appl. Phys. Lett.*, 2014, **105**, 183902.

31 R. He, C. Zuo, S. Ren, D. Zhao and L. Ding, Low-Bandgap Sn–Pb Perovskite Solar Cells, *J. Semicond.*, 2021, **42**, 060202.

32 J. Park, J. Kim, H.-S. Yun, M. J. Paik, E. Noh, H. J. Mun, M. G. Kim, T. J. Shin and S. Il Seok, Controlled Growth of Perovskite Layers with Volatile Alkylammonium Chlorides, *Nature*, 2023, **616**, 724–730.

33 J. Jeong, M. Kim, J. Seo, H. Lu, P. Ahlawat, A. Mishra, Y. Yang, M. A. Hope, F. T. Eickemeyer, M. Kim, Y. J. Yoon, I. W. Choi, B. P. Darwich, S. J. Choi, Y. Jo, J. H. Lee,

B. Walker, S. M. Zakeeruddin, L. Emsley, U. Rothlisberger, A. Hagfeldt, D. S. Kim, M. Grätzel and J. Y. Kim, Pseudo-Halide Anion Engineering for α-FAPbI₃ Perovskite Solar Cells, *Nature*, 2021, **592**, 381–385.

34 Y. Bai, Z. Huang, X. Zhang, J. Lu, X. Niu, Z. He, C. Zhu, M. Xiao, Q. Song, X. Wei, C. Wang, Z. Cui, J. Dou, Y. Chen, F. Pei, H. Zai, W. Wang, T. Song, P. An, J. Zhang, J. Dong, Y. Li, J. Shi, H. Jin, P. Chen, Y. Sun, Y. Li, H. Chen, Z. Wei, H. Zhou and Q. Chen, Initializing Film Homogeneity to Retard Phase Segregation for Stable Perovskite Solar Cells, *Science*, 2022, **378**, 747–754.

35 R. Azmi, E. Ugur, A. Seitkhan, F. Aljamaan, A. S. Subbiah, J. Liu, G. T. Harrison, M. I. Nugraha, M. K. Eswaran, M. Babics, Y. Chen, F. Xu, T. G. Allen, A. ur Rehman, C.-L. Wang, T. D. Anthopoulos, U. Schwingenschlögl, M. De Bastiani, E. Aydin and S. De Wolf, Damp Heat–Stable Perovskite Solar Cells with Tailored-Dimensionality 2D/3D Heterojunctions, *Science*, 2022, **376**, 73–77.

36 N. Liu, P. Liu, H. Zhou, Y. Bai and Q. Chen, Understanding the Defect Properties of Quasi-2D Halide Perovskites for Photovoltaic Applications, *J. Phys. Chem. Lett.*, 2020, **11**, 3521–3528.

37 N. Liu, P. Liu, H. Ren, H. Xie, N. Zhou, Y. Gao, Y. Li, H. Zhou, Y. Bai and Q. Chen, Probing Phase Distribution in 2D Perovskites for Efficient Device Design, *ACS Appl. Mater. Interfaces*, 2020, **12**, 3127–3133.

38 Z. Zhu, Y. Bai, T. Zhang, Z. Liu, X. Long, Z. Wei, Z. Wang, L. Zhang, J. Wang, F. Yan and S. Yang, High-Performance Hole-Extraction Layer of Sol–Gel-Processed NiO Nanocrystals for Inverted Planar Perovskite Solar Cells, *Angew. Chem., Int. Ed.*, 2014, **53**, 12571–12575.

39 D. P. McMeekin, G. Sadoughi, W. Rehman, G. E. Eperon, M. Saliba, M. T. Hörantner, A. Haghighirad, N. Sakai, L. Korte, B. Rech, M. B. Johnston, L. M. Herz and H. J. Snaith, A Mixed-Cation Lead Mixed-Halide Perovskite Absorber for Tandem Solar Cells, *Science*, 2016, **351**, 151–155.

40 Z. Qiu, N. Li, Z. Huang, Q. Chen and H. Zhou, Recent Advances in Improving Phase Stability of Perovskite Solar Cells, *Small Methods*, 2020, **4**, 1900877.

41 Y. Guo, K. Shoyama, W. Sato, Y. Matsuo, K. Inoue, K. Harano, C. Liu, H. Tanaka and E. Nakamura, Chemical Pathways Connecting Lead(ɪɪ) Iodide and Perovskite *via* Polymeric Plumbate(ɪɪ) Fiber, *J. Am. Chem. Soc.*, 2015, **137**, 15907–15914.

42 Z. Li, Y. Sun, H. Yao, J. Zhao, Q. Wang, L. Ding and Z. Jin, Intermediates Transformation for Efficient Perovskite Solar Cells, *J. Energy Chem.*, 2021, **52**, 102–114.

43 X. Huang, F. Cheng, B. Wu and N. Zheng, Intermediate Chemistry of Halide Perovskites: Origin, Evolution, and Application, *J. Phys. Chem. Lett.*, 2022, **13**, 1765–1776.

44 G. Yin, H. Zhao, H. Jiang, S. Yuan, T. Niu, K. Zhao, Z. Liu and S. (Frank) Liu, Precursor Engineering for All-Inorganic CsPbI₂Br Perovskite Solar Cells with 14.78% Efficiency, *Adv. Funct. Mater.*, 2018, **28**, 1803269.

45 H. Jiang, J. Feng, H. Zhao, G. Li, G. Yin, Y. Han, F. Yan, Z. Liu and S. (Frank) Liu, Low Temperature Fabrication for High Performance Flexible CsPbI₂Br Perovskite Solar Cells., *Adv. Sci.*, 2018, **5**, 1801117.

46 S. Yang, J. Wen, Z. Liu, Y. Che, J. Xu, J. Wang, D. Xu, N. Yuan, J. Ding, Y. Duan and S. Liu, A Key 2D Intermediate Phase for Stable High-Efficiency CsPbI₂Br Perovskite Solar Cells, *Adv. Energy Mater.*, 2022, **12**, 2103019.

47 W. Budiawan, H. C. Chen, A. Mohapatra, A. Singh, P. C. Wang, K. T. Wong and C. W. Chu, Core-Twisted Tetrachloroperylenediimide Additives Improve the Crystallinity of Perovskites to Provide Efficient Perovskite Solar Cells, *Sol. Energy Mater. Sol. Cells*, 2022, **243**, 111779.

48 F. Li, X. Huang, J. Xue, F. Liu, D. Kim, H. S. Yang, E. Yang, I. Shin, J. Kim, B. R. Lee and S. H. Park, Effective Multifunctional Additive Engineering for Efficient and Stable Inverted Perovskite Solar Cells, *Sol. RRL*, 2022, **6**, 2200645.

49 J. Zhang, L. Zhang, X. Li, X. Zhu, J. Yu and K. Fan, Binary Solvent Engineering for High-Performance Two-Dimensional Perovskite Solar Cells, *ACS Sustainable Chem. Eng.*, 2019, **7**, 3487–3495.

50 F. Yu, J. Liu, J. Huang, P. Xu, C. H. Li, Y. X. Zheng, H. Tan and J. L. Zuo, Efficient and Stable Wide-Bandgap Perovskite Solar Cells Derived from a Thermodynamic Phase-Pure Intermediate, *Sol. RRL*, 2022, **6**, 2100906.

51 F. Z. Qiu, M. H. Li, S. Wang, J. Y. Sun, Y. Jiang, J. J. Qi and J. S. Hu, Regulating the Crystalline Phase of Intermediate Films Enables FA₁₋ₓMAₓPbI₃ Perovskite Solar Cells with Efficiency over 22%, *J. Mater. Chem. A*, 2021, **9**, 24064–24070.

52 G. Wang, L. Wang, J. Qiu, Z. Yan, K. Tai, W. Yu and X. Jiang, Fabrication of Efficient Formamidinium Perovskite Solar Cells under Ambient Air *via* Intermediate-Modulated Crystallization, *Sol. Energy*, 2019, **187**, 147–155.

53 J. Wang, L. Yuan, H. Luo, C. Duan, B. Zhou, Q. Wen and K. Yan, Ambient Air Processed Highly Oriented Perovskite Solar Cells with Efficiency Exceeding 23% *via* Amorphous Intermediate, *Chem. Eng. J.*, 2022, **446**, 136968.

54 Y. Ge, H. Wang, C. Wang, C. Wang, H. Guan, W. Shao, T. Wang, W. Ke, C. Tao and G. Fang, Intermediate Phase Engineering with 2,2-Azodi(2-Methylbutyronitrile) for Efficient and Stable Perovskite Solar Cells, *Adv. Mater.*, 2023, **35**, 2210186.

55 D. P. McMeekin, P. Holzhey, S. O. Fürer, S. P. Harvey, L. T. Schelhas, J. M. Ball, S. Mahesh, S. Seo, N. Hawkins, J. Lu, M. B. Johnston, J. J. Berry, U. Bach and H. J. Snaith, Intermediate-phase engineering *via* dimethylammonium cation additive for stable perovskite solar cells, *Nat. Mater.*, 2023, **22**, 73–83.

56 F. Li, X. Deng, Z. Shi, S. Wu, Z. Zeng, D. Wang, Y. Li, F. Qi, Z. Zhang, Z. Yang, S. H. Jang, F. R. Lin, S.-W. Tsang, X. K. Chen and A. K. Y. Jen, Hydrogen-bond-bridged intermediate for perovskite solar cells with enhanced efficiency and stability, *Nat. Photonics*, 2023, **17**, 478–484.

57 B. Wang, Q. Cheng, G. Huang, Y. Yue, W. Zhang, X. Li, Y. Li, W. Du, X. Liu, H. Zhang, Y. Zhang and H. Zhou, Sulfonium-Cations-Assisted Intermediate Engineering for

Quasi-2D Perovskite Solar Cells, *Adv. Mater.*, 2023, **35**, 2207345.

58 J. Xu, Q. Wu, Y. He, M. Cui, H. Han, H. Liu and J. Yao, Efficient two-dimensional $Cs_2PbI_2(SCN)_2$ perovskite solar cells *via* intermediate-modulated crystallization, *J. Mater. Chem. A*, 2023, **11**, 5380–5389.

59 Y. Yang, Y. Wang, Z. Qu, K. Zhang, T. Liang, S. Chen, W. Lv, F. Min, Y. Chen, Y. Qiao and Y. Song, Volatile Dual-Solvent Assisted Intermediate Phase Regulation for Anti-Solvent-Free Perovskite Photovoltaics, *Angew. Chem., Int. Ed.*, 2023, **62**, e202300971.

60 S. Tang, J. Zong, Z. Zhu, Z. Wang, W. Pan, L. Zhao, R. Chen and M. Li, Kinetic Control of Solvate Intermediate Evolution for High-Performance Perovskite Solar Cells by the Facial Mask Incubation Technique, *ACS Appl. Mater. Interfaces*, 2023, **15**, 21171–21178.

61 H. Wang, H. Liu, Z. Dong, X. Wei, Y. Song, W. Li, L. Zhu, Y. Bai and H. Chen, Extracting Ammonium Halides by Solvent from the Hybrid Perovskites with Various Dimensions to Promote the Crystallization of $CsPbI_3$ Perovskite., *Nano Energy*, 2022, **94**, 106925.

62 E. L. Lim, J. Yang and Z. Wei, Inorganic $CsPbI_2Br$ Halide Perovskites: From Fundamentals to Solar Cell Optimizations, *Energy Environ. Sci.*, 2023, **16**, 862–888.

63 C. Sun, P. Yang, Z. Nan, C. Tian, Y. Cai, J. Chen, F. Qi, H. Tian, L. Xie, L. Meng and Z. Wei, Well-Defined Fullerene Bis adducts Enable High-Performance Tin-Based Perovskite Solar Cells, *Adv. Mater.*, 2023, **35**, 2205603.

64 D. He, L. Shen, Y. Bai and L. Wang, Rational Strategies toward Efficient and Stable Lead-Free Tin Halide Perovskite Solar Cells, *Mater. Chem. Front.*, 2021, **5**, 4107–4127.

65 H. Wang, H. Liu, Z. Dong, W. Li, L. Zhu and H. Chen, Composition Manipulation Boosts the Efficiency of Carbon-Based $CsPbI_3$ Perovskite Solar Cells to beyond 14%, *Nano Energy*, 2021, **84**, 105881.

66 Y. C. Zheng, S. Yang, X. Chen, Y. Chen, Y. Hou and H. G. Yang, Thermal-Induced Volmer–Weber Growth Behavior for Planar Heterojunction Perovskite Solar Cells, *Chem. Mater.*, 2015, **27**, 5116–5121.

67 L. Lou, T. Liu, J. Xiao, S. Xiao, X. Long, S. Zheng and S. Yang, Controlling Apparent Coordinated Solvent Number in the Perovskite Intermediate Phase Film for Developing Large-Area Perovskite Solar Modules, *Energy Technol.*, 2020, **8**, 1900972.

68 H. Yao, J. Zhao, Z. Li, Z. Ci and Z. Jin, Research and Progress of Black Metastable Phase $CsPbI_3$ Solar Cells, *Mater. Chem. Front.*, 2021, **5**, 1221–1235.

69 J. Ren, G. Zhai, Q. Chen, Z. Wu, B. Wang, Y. Huo, C. Yu and B. Xu, Effect of Reaction Temperature on Film Quality and Cell Performance: Comparative Study of Single and Mixed Cation/Halide Perovskites, *Mater. Sci. Semicond. Process.*, 2022, **446**, 136968.

70 M. Kim, G. H. Kim, K. S. Oh, Y. Jo, H. Yoon, K. H. Kim, H. Lee, J. Y. Kim and D. S. Kim, High-Temperature-Short-Time Annealing Process for High-Performance Large-Area Perovskite Solar Cells, *ACS Nano*, 2017, **11**, 6057–6064.

71 H. J. Lee, Y. H. Seo, S. S. Kim and S. I. Na, Slot-Die Processed Perovskite Solar Cells: Effects of Solvent and Temperature on Device Performances, *Semicond. Sci. Technol.*, 2022, **37**, 045007.

72 S. Du, J. Yang, S. Qu, Z. Lan, T. Sun, Y. Dong, Z. Shang, D. Liu, Y. Yang, L. Yan, X. Wang, H. Huang, J. Ji, P. Cui, Y. Li and M. Li, Impact of Precursor Concentration on Perovskite Crystallization for Efficient Wide-Bandgap Solar Cells, *Materials*, 2022, **15**, 3185.

73 Y. Du, P. Liu, F. Li, X. Hou, H. Zhang, Y. Shi, S. Wang, Y. Wang, S. Guo, Q. Tai and X. Zhao, Precursor Engineering for Performance Enhancement of Hole-Transport-Layer-Free Carbon-Based $MAPbBr_3$ Perovskite Solar Cells, *J. Alloys Compd.*, 2020, **832**, 154902.

74 F. Xu, Y. Zou, Y. Dai, M. Li and Z. Li, Halide perovskites and high-pressure technologies: a fruitful encounter, *Mater. Chem. Front.*, 2023, **7**, 2102–2119.

75 J. Luo, J. Xia, H. Yang, C. Sun, N. Li, H. A. Malik, H. Shu, Z. Wan, H. Zhang, C. J. Brabec and C. Jia, A Pressure Process for Efficient and Stable Perovskite Solar Cells, *Nano Energy*, 2020, **77**, 105063.

76 M. Liu and T. Pauporté, Additive Engineering for Stable and Efficient Dion–Jacobson Phase Perovskite Solar Cells, *Nano-Micro Lett.*, 2020, **10**, 1902.

77 Y. Yin, Y. Zhou, S. Fu, X. Zuo, Y. Lin, L. Wang, Y. Xue, Y. Zhang, E. H. R. Tsai, S. Hwang, K. Kissenger, M. Li, M. Cotlet, T. Li, K. G. Yager, C. Nam and M. H. Rafailovich, Enhancing Crystallization in Hybrid Perovskite Solar Cells Using Thermally Conductive 2D Boron Nitride Nanosheet Additive, *Small*, 2023, **19**, 2207092.

78 L. A. Castriotta, E. Calabrò, F. Di Giacomo, S. H. Reddy, D. Takhellambam, B. Paci, A. Generosi, L. Serenelli, F. Menchini, L. Martini, M. Tucci and A. Di Carlo, A universal multi-additive strategy to enhance efficiency and stability in inverted perovskite solar cells, *Nano Energy*, 2023, **109**, 108268.

79 R. Zhuang, L. Wang, J. Qiu, L. Xie, X. Miao, X. Zhang and Y. Hua, Effect of molecular configuration of additives on perovskite crystallization and hot carriers behavior in perovskite solar cells, *Chem. Eng. J.*, 2023, **463**, 142449.

80 L. Meng, Q. Wei, Z. Yang, D. Yang, J. Feng, X. Ren, Y. Liu and S. (Frank) Liu, Improved Perovskite Solar Cell Efficiency by Tuning the Colloidal Size and Free Ion Concentration in Precursor Solution Using Formic Acid Additive, *J. Energy Chem.*, 2020, **41**, 43–51.

81 W. Zhao, J. Xu, K. He, Y. Cai, Y. Han, S. Yang, S. Zhan, D. Wang, Z. Liu and S. Liu, A Special Additive Enables All Cations and Anions Passivation for Stable Perovskite Solar Cells with Efficiency over 23%, *Nano-Micro Lett.*, 2021, **13**, 169.

82 L. Li, X. Xu, L. Xiao, W. Jiang, J. Zhao, X. Kong and G. Zou, Symmetrical Conjugated Molecular Additive for Defect Passivation and Charge Transfer Bridge in Perovskite Solar Cells, *ACS Appl. Energy Mater.*, 2021, **4**, 5935–5943.

83 L. Ning, L. Song, X. Wen, N. Gu, P. Du, J. Yu and J. Xiong, Enhanced Molecular Interaction by Polymer Additive for

Efficient and Stable Flexible Perovskite Solar Cells, *J. Mater. Sci.*, 2022, **57**, 20654–20671.

84 C. Zhang, X. Wan, J. Zang, Q. Liu, Y. Fei and Z. Yu, Polymer-Modified CsPbI$_2$Br Films for All-Inorganic Planar Perovskite Solar Cells with Improved Performance, *Surf. Interfaces*, 2021, **22**, 100809.

85 M. Zhong, L. Chai, Y. Wang and J. Di, Enhanced Efficiency and Stability of Perovskite Solar Cell by Adding Polymer Mixture in Perovskite Photoactive Layer, *J. Alloys Compd.*, 2021, **864**, 158793.

86 S. Shaik, Z. Zhou, Z. Ouyang, R. Han and D. Li, Polymer Additive Assisted Fabrication of Compact and Ultra-Smooth Perovskite Thin Films with Fast Lamp Annealing, *Energies*, 2021, **14**, 2656.

87 S. Narendhiran, A. Kunka Ravindran, I. D. Rajan Thomas, S. P. Muthu and R. Perumalsamy, Poly(Vinylidene Fluoride-Co-Hexafluoropropylene) Additive in Perovskite for Stable Performance of Carbon-Based Perovskite Solar Cells, *Int. J. Energy Res.*, 2022, **46**, 1565–1574.

88 M. C. Wu, Y. Y. Li, S. H. Chan, K. M. Lee and W. F. Su, Polymer Additives for Morphology Control in High-Performance Lead-Reduced Perovskite Solar Cells, *Sol. RRL*, 2020, **4**, 2070063.

89 Y. He, Z. Lin, J. Wang, K. Zhang, X. Xu, Y. Li, X. Huang, T. Ma, S. Xiao and S. Yang, A Heat-Liquefiable Solid Precursor for Ambient Growth of Perovskites with High Tunability, Performance and Stability, *Small Methods*, 2022, **6**, 2200384.

90 W. Zhao, J. Xu, K. He, Y. Cai, Y. Han, S. Yang, S. Zhan, D. Wang, Z. Liu and S. Liu, A Special Additive Enables All Cations and Anions Passivation for Stable Perovskite Solar Cells with Efficiency over 23%, *Nano-Micro Lett.*, 2021, **13**, 169.

91 Q. Wang, W. Tang, Y. Chen, W. Qiu, Y. Wu and Q. Peng, Over 25% Efficiency and Stable Bromine-Free RbCsFAMA-Based Quadruple Cation Perovskite Solar Cells Enabled by an Aromatic Zwitterion, *J. Mater. Chem. A*, 2022, **11**, 1170–1179.

92 Y. Zhang, Y. Li, L. Zhang, H. Hu, Z. Tang, B. Xu and N. G. Park, Propylammonium Chloride Additive for Efficient and Stable FAPbI$_3$ Perovskite Solar Cells, *Adv. Energy Mater.*, 2021, **11**, 2102538.

93 S. Tan, J. Shi, B. Yu, W. Zhao, Y. Li, Y. Li, H. Wu, Y. Luo, D. Li and Q. Meng, Inorganic Ammonium Halide Additive Strategy for Highly Efficient and Stable CsPbI$_3$ Perovskite Solar Cells, *Adv. Funct. Mater.*, 2021, **31**, 2010813.

94 S. Sandhu, R. Singh, K. Yoo, M. Kumar and J. J. Lee, Effect of Binary Additives in Mixed 2D/3D Sn-Based Perovskite Solar Cells, *J. Power Sources*, 2021, **491**, 229574.

95 J. Jeong, M. Kim, J. Seo, H. Lu, P. Ahlawat, A. Mishra, Y. Yang, M. A. Hope, F. T. Eickemeyer, M. Kim, Y. J. Yoon, I. W. Choi, B. P. Darwich, S. J. Choi, Y. Jo, J. H. Lee, B. Walker, S. M. Zakeeruddin, L. Emsley, U. Rothlisberger, A. Hagfeldt, D. S. Kim, M. Grätzel and J. Y. Kim, Pseudo-Halide Anion Engineering for α-FAPbI$_3$ Perovskite Solar Cells, *Nature*, 2021, **592**, 381–385.

96 X. Tang, S. Yi, Q. Yuan, Q. Shu, D. Han and L. Feng, 2D Non-Layered In$_2$S$_3$ as Multifunctional Additive for Inverted Organic-Free Perovskite Solar Cells with Enhanced Performance, *Sol. RRL*, 2022, **6**, 2101013.

97 G. Li, X. Zou, J. Cheng, D. Chen, Y. Yao, C. Chang, X. Yu, Z. Zhou, J. Wang and B. Liu, Impact of Perovskite Composition on Film Formation Quality and Photophysical Properties for Flexible Perovskite Solar Cells, *Molecules*, 2020, **25**, 732.

98 Z. Li, J. Feng, J. Cao, J. Jin, Y. Zhou, D. Cao, Z. Liang, B. Zhu, M. Li, L. Zhao and S. Wang, New Carbon Nitride C$_3$N$_4$ Additive for Improving Cationic Defects of Perovskite Solar Cells, *Energy Environ. Mater.*, 2023, **6**, e12283.

99 H. Zai, Y. Ma, Q. Chen and H. Zhou, Ion Migration in Halide Perovskite Solar Cells: Mechanism, Characterization, Impact and Suppression, *J. Energy Chem.*, 2021, **63**, 528–549.

100 Y. Wang, C. Jia, Z. Fan, Z. Lin, S.-J. Lee, T. L. Atallah, J. R. Caram, Y. Huang and X. Duan, Large-Area Synthesis and Patterning of All-Inorganic Lead Halide Perovskite Thin Films and Heterostructures, *Nano Lett.*, 2021, **21**, 1454–1460.

101 I. Karimata and T. Tachikawa, *In Situ* Exploration of the Structural Transition during Morphology- and Efficiency-Conserving Halide Exchange on a Single Perovskite Nanocrystal, *Angew. Chem., Int. Ed.*, 2021, **60**, 2548–2553.

102 A. Haque, V. K. Ravi, G. S. Shanker, I. Sarkar, A. Nag and P. K. Santra, Internal Heterostructure of Anion-Exchanged Cesium Lead Halide Nanocubes, *J. Phys. Chem. C*, 2018, **122**, 13399–13406.

103 Q. A. Akkerman, V. D'Innocenzo, S. Accornero, A. Scarpellini, A. Petrozza, M. Prato and L. Manna, Tuning the Optical Properties of Cesium Lead Halide Perovskite Nanocrystals by Anion Exchange Reactions, *J. Am. Chem. Soc.*, 2015, **137**, 10276–10281.

104 Y. Hu, J. Schlipf, M. Wussler, M. L. Petrus, W. Jaegermann, T. Bein, P. Müller-Buschbaum and P. Docampo, Hybrid Perovskite/Perovskite Heterojunction Solar Cells, *ACS Nano*, 2016, **10**, 5999–6007.

105 M. He, J. Liang, Z. Zhang, Y. Qiu, Z. Deng, H. Xu, J. Wang, Y. Yang, Z. Chen and C.-C. Chen, Compositional Optimization of a 2D–3D Heterojunction Interface for 22.6% Efficient and Stable Planar Perovskite Solar Cells, *J. Mater. Chem. A*, 2020, **8**, 25831–25841.

106 C. Chen, Z. Song, C. Xiao, D. Zhao, N. Shrestha, C. Li, G. Yang, F. Yao, X. Zheng, R. J. Ellingson, C.-S. Jiang, M. Al-Jassim, K. Zhu, G. Fang and Y. Yan, Achieving a High Open-Circuit Voltage in Inverted Wide-Bandgap Perovskite Solar Cells with a Graded Perovskite Homojunction, *Nano Energy*, 2019, **61**, 141–147.

107 S. Gharibzadeh, B. Abdollahi Nejand, M. Jakoby, T. Abzieher, D. Hauschild, S. Moghadamzadeh, J. A. Schwenzer, P. Brenner, R. Schmager, A. A. Haghighirad, L. Weinhardt, U. Lemmer, B. S. Richards, I. A. Howard and U. W. Paetzold, Record Open-Circuit Voltage Wide-Bandgap Perovskite Solar Cells Utilizing 2D/3D Perovskite Heterostructure, *Adv. Energy Mater.*, 2019, **9**, 1803699.

108 F. Li, X. Hou, Z. Wang, X. Cui, G. Xie, F. Yan, X. Z. Zhao and Q. Tai, FA/MA Cation Exchange for Efficient and Reproducible Tin-Based Perovskite Solar Cells, *ACS Appl. Mater. Interfaces*, 2021, **13**, 40656–40663.

109 G. Jeong, D. Koo, J. H. Woo, Y. Choi, E. Son, F. Huang, J. Y. Kim and H. Park, Highly Efficient Self-Encapsulated Flexible Semitransparent Perovskite Solar Cells *via* Bifacial Cation Exchange, *ACS Appl. Mater. Interfaces*, 2022, **14**(29), 33297–33305.

110 Z. Shao, H. Meng, X. Du, X. Sun, P. Lv, C. Gao, Y. Rao, C. Chen, Z. Li, X. Wang, G. Cui and S. Pang, Cs_4PbI_6-Mediated Synthesis of Thermodynamically Stable $FA_{0.15}$–$Cs_{0.85}PbI_3$ Perovskite Solar Cells, *Adv. Mater.*, 2020, **32**, 2001054.

111 Y. Miao, H. Fan, P. Wang, Y. Zhang, C. Gao, L. M. Yang, Y. L. Song, C. Yang, C. M. Liu and K. J. Jiang, From 1D to 3D: Fabrication of $CH_3NH_3PbI_3$ Perovskite Solar Cell Thin Films from (Pyrrolidinium)PbI_3 *via* Organic Cation Exchange Approach, *Energy Technol.*, 2020, **8**, 2000148.

112 C. F. J. Lau, Z. Wang, N. Sakai, J. Zheng, C. H. Liao, M. Green, S. Huang, H. J. Snaith and A. Ho-Baillie, Fabrication of Efficient and Stable $CsPbI_3$ Perovskite Solar Cells through Cation Exchange Process, *Adv. Energy Mater.*, 2019, **9**, 1901685.

113 C. Niu, C. Wang, G. Zhang, Q. Zhao, C. Fang, W. Li, F. Huang, Z. Ku and Y. Cheng, High-Performance Rb–$Cs_{0.14}FA_{0.86}Pb(Br_xI_{1-x})_3$ Perovskite Solar Cells Achieved by Regulating the Halogen Exchange in Vapor–Solid Reaction Process, *Sol. RRL*, 2021, **5**, 2100102.

114 B. Ding, J. Peng, Q.-Q. Chu, S. Zhao, H. Shen, K. J. Weber, G.-J. Yang, T. P. White, K. R. Catchpole, M. K. Nazeeruddin and P. J. Dyson, Anion Exchange-Induced Crystal Engineering *via* Hot-Pressing Sublimation Affording Highly Efficient and Stable Perovskite Solar Cells, *Sol. RRL*, 2021, **5**, 2000729.

115 Z. Zhang, D. Chen, W. Zhu, J. Ma, W. Chai, D. Chen, J. Zhang, C. Zhang and Y. Hao, Slow Halide Exchange in $CsPbIBr_2$ Films for High-Efficiency, Carbon-Based, All-Inorganic Perovskite Solar Cells, *Sci. China Mater.*, 2021, **64**, 2107–2117.

116 H. Wu, A. Erbing, M. B. Johansson, J. Wang, C. Kamal, M. Odelius and E. M. J. Johansson, Mixed-Halide Double Perovskite Cs_2AgBiX_6 (X = Br, I) with Tunable Optical Properties *via* Anion Exchange, *ChemSusChem*, 2021, **14**, 4507–4515.

117 X. Jiao, W.-M. Gu, Y. Xu, K.-J. Jiang, G. Yu, Q.-W. Zhang, C.-Y. Gao, C.-M. Liu, X.-H. Fan, L.-M. Yang and Y. Song, Anion-Exchange Assisted Sequential Deposition for Stable and Efficient $FAPbI_3$-Based Perovskite Solar Cells, *Chem. Eng. J.*, 2023, **452**, 139326.

118 S. Shan, C. Xu, H. Wu, B. Niu, W. Fu, L. Zuo and H. Chen, Manipulating the Crystallization and Phase Transition for High-Performance $CsPbI_2Br$ Solar Cells, *Adv. Energy Mater.*, 2023, **13**, 2203682.

119 M. Liu, M. B. Johnston and H. J. Snaith, Efficient Planar Heterojunction Perovskite Solar Cells by Vapour Deposition, *Nature*, 2013, **501**, 395–398.

120 V. Arivazhagan, J. Xie, Z. Yang, P. Hang, M. M. Parvathi, K. Xiao, C. Cui, D. Yang and X. Yu, Vacuum Co-Deposited $CH_3NH_3PbI_3$ Films by Controlling Vapor Pressure for Efficient Planar Perovskite Solar Cells, *Sol. Energy*, 2019, **181**, 339–344.

121 L. Gil-Escrig, C. Dreessen, F. Palazon, Z. Hawash, E. Moons, S. Albrecht, M. Sessolo and H. J. Bolink, Efficient Wide-Bandgap Mixed-Cation and Mixed-Halide Perovskite Solar Cells by Vacuum Deposition, *ACS Energy Lett.*, 2021, **6**, 827–836.

122 A. Babaei, W. Soltanpoor, M. A. Tesa-Serrate, S. Yerci, M. Sessolo and H. J. Bolink, Preparation and Characterization of Mixed Halide $MAPbI_{3-x}Cl_x$ Perovskite Thin Films by Three-Source Vacuum Deposition, *Energy Technol.*, 2020, **8**, 1900784.

123 J. Yin, H. Qu, J. Cao, H. Tai, J. Li and N. Zheng, Vapor-Assisted Crystallization Control toward High Performance Perovskite Photovoltaics with over 18% Efficiency in the Ambient Atmosphere, *J. Mater. Chem. A*, 2016, **4**, 13203–13210.

124 M. M. Tavakoli, Z. Fazel, R. Tavakoli, S. Akin, S. Satapathi, D. Prochowicz and P. Yadav, Efficient and Less-Toxic Indium-Doped $MAPbI_3$ Perovskite Solar Cells Prepared by Metal Alloying Technique, *Sol. RRL*, 2022, **6**, 2200106.

125 G. Tong, H. Li, G. Li, T. Zhang, C. Li, L. Yu, J. Xu, Y. Jiang, Y. Shi and K. Chen, Mixed Cation Perovskite Solar Cells by Stack-Sequence Chemical Vapor Deposition with Self-Passivation and Gradient Absorption Layer, *Nano Energy*, 2018, **48**, 536–542.

126 Y. Wang, T. Wu, J. Barbaud, W. Kong, D. Cui, H. Chen, X. Yang and L. Han, Stabilizing heterostructures of soft perovskite semiconductors, *Science*, 2019, **365**, 687–691.

127 X. Lin, H. Su, S. He, Y. Song, Y. Wang, Z. Qin, Y. Wu, X. Yang, Q. Han, J. Fang, Y. Zhang, H. Segawa, M. Grätzel and L. Han, *In situ* growth of graphene on both sides of a Cu–Ni alloy electrode for perovskite solar cells with improved stability, *Nat. Energy*, 2022, **7**, 520–527.